



**HAL**  
open science

## Temperature-dependent mechanisms of the atmospheric alteration of a mixed-alkali lime silicate glass

Fanny Alloteau, Odile Majérus, Isabelle Biron, Patrice Lehuédé, Daniel Caurant, Thibault Charpentier, Antoine Seyeux

► **To cite this version:**

Fanny Alloteau, Odile Majérus, Isabelle Biron, Patrice Lehuédé, Daniel Caurant, et al.. Temperature-dependent mechanisms of the atmospheric alteration of a mixed-alkali lime silicate glass. *Corrosion Science*, 2019, 159 (108129), pp.108129. 10.1016/j.corsci.2019.108129 . cea-02265811

**HAL Id: cea-02265811**

**<https://cea.hal.science/cea-02265811>**

Submitted on 20 Dec 2021

**HAL** is a multi-disciplinary open access archive for the deposit and dissemination of scientific research documents, whether they are published or not. The documents may come from teaching and research institutions in France or abroad, or from public or private research centers.

L'archive ouverte pluridisciplinaire **HAL**, est destinée au dépôt et à la diffusion de documents scientifiques de niveau recherche, publiés ou non, émanant des établissements d'enseignement et de recherche français ou étrangers, des laboratoires publics ou privés.



Distributed under a Creative Commons Attribution - NonCommercial 4.0 International License

# 1 Temperature-dependent mechanisms of the atmospheric alteration 2 of a mixed-alkali lime silicate glass

3  
4 Fanny Alloteau<sup>a,b</sup>, Odile Majérous<sup>b</sup>, Isabelle Biron<sup>a</sup>, Patrice Lehuédé<sup>a</sup>, Daniel Caurant<sup>b</sup>, Thibault  
5 Charpentier<sup>c</sup>, Antoine Seyeux<sup>b</sup>

6  
7 <sup>a</sup> Centre de Recherche et de Restauration des Musées de France (C2RMF), F-75001 Paris, France

8 <sup>b</sup> PSL University, Chimie Paristech, CNRS, Institut de Recherche de Chimie Paris, F-75005 Paris,  
9 France

10 <sup>c</sup> NIMBE, CEA, CNRS, Université Paris-Saclay, CEA Saclay, F-91191, Gif-sur-Yvette, France

11

## 12 Abstract

13 The atmospheric alteration of a mixed-alkali lime silicate glass is described as a function of time  
14 and temperature. The glass hydration kinetics self-accelerates with time and is considerably  
15 enhanced with the temperature. At 80°C, alkali and alkaline earth ions are retained in hydrate-  
16 type environments while at 40°C, they are partially leached out forming surface carbonates, in the  
17 order  $\text{Ca}^{2+} > \text{Na}^{+} > \text{K}^{+}$ . The temperature dependency of hydrolysis processes, the important role  
18 of the hydration energy of cations and the diminished solvation properties of bound water are  
19 considered to discuss experimental observations and advance in the understanding of the  
20 specificities of glass atmospheric alteration.

21

## 22 1. INTRODUCTION

23 Glass is a unique material made by melting silica (from sand) with a flux: an alkali and/or  
24 alkaline-earth bearing agent that will lower the melt temperature and viscosity. Because of their  
25 relatively alkali-rich composition, glasses are more prone to environmental degradation than  
26 other oxide-based materials such as traditional ceramics. The degradation always involves the  
27 reaction of glass with water, but the physical, chemical and mass transport conditions determine  
28 the extent and result of the process. In this paper, atmospheric alteration refers to the  
29 degradation of glass by water in the atmosphere (*ie* when relative humidity, RH, is <100%). In the  
30 field of Cultural Heritage, this condition excludes, for instance, the water condensation and rain  
31 water running off experienced by stained glass windows [1,2] or the saturated environment of  
32 buried archaeological objects [3]. Specifically, it is the condition of glasses conserved in  
33 atmosphere in the museums, with their diverse nature (glass objects, glazes and enamels).  
34 Although this condition is commonly considered as mild, it can give rise to significant damage

35 depending on the glass composition and climatic conditions (temperature, relative humidity,  
36 atmospheric pollutants) [4–8] and it is an issue for curators to be able to identify stable from  
37 unstable compositions and adjust the environmental parameters to protect the more alterable  
38 pieces [5,9–13]. Atmospheric alteration of glass causes short-term issues also in the glass industry,  
39 every time that glass is stored in confined in wet conditions ( $RH > 70\%$ ) [14,15]. The  
40 consequences of the surface defects induced by the alteration are the reduction of mechanical  
41 properties of glass containers or the degradation of the quality of the thin coatings deposited on  
42 float glass [16,17]. Recently, glass atmospheric alteration has become an important matter of  
43 concern in the assessment of the long-term safety of geological repository of nuclear waste  
44 glasses [18–20]. Indeed, it is estimated that the nuclear glass will be exposed to undersaturated  
45 conditions for thousands of years [20].

46 The manifestations of the atmospheric alteration of glass are very specific, and after several  
47 centuries of their description, specific and well-defined terms have emerged and been accepted in  
48 both the scientific and conservation communities, the most characteristic one being “crizzling”  
49 [4]. In particular, Brill [7,10] and Koob [5,11] have identified and accurately described several  
50 successive stages of this deterioration that can overlap and be more or less rapid according to  
51 both the glass composition and the storage conditions : (i) In an initial stage, alkali salts form on  
52 the surface and give to the glass a hazy or cloudy appearance. (ii) In the second stage called  
53 incipient crizzling, microcracks of the glass surface appear but they are visible under a  
54 microscope only. (iii) In the third stage called full-blown crizzling, the cracking of the glass has  
55 grown deeper below the surface and a uniform network of cracks becomes visible to the naked  
56 eye. (iv) At the advanced stage of crizzling, flakes fall down from the deeply cracked surface.  
57 Eventually, the whole glass piece may desaggregate. Note that the appearance of alkali and calcium  
58 salts (carbonates or sulfates) forming a hazy veil on the glass surface, is also observed as an initial  
59 stage of the atmospheric degradation of industrial soda-lime glasses [14,16,21,22]. Surface  
60 cracking is even reported in the most severe conditions ( $RH = 70\%$  and  $80\%$ ) [22].

61 These manifestations correspond to the ambient temperature phenomena ( $0 < T < 50^{\circ}\text{C}$ ). The  
62 general mechanisms are relatively well understood [5,21,23,24]: under a wet atmosphere ( $RH >$   
63  $60\text{-}70\%$ ), alkali are leached out of the glass surface and precipitate with acid gases in the adsorbed  
64 water film. The alkali-depleted and hydrated leached layer, well observed in numerous studies,  
65 has different molar volume and thermal expansion coefficient than the bulk glass, causing its  
66 cracking under the effect of cycling temperature and RH, after the layer thickness has reached  
67 some threshold. By water diffusion through the leached layer or in the cracks, the alteration  
68 progresses and the hydrated layer grows.

69 Beyond this general picture, numerous questions arise regarding the detailed mechanisms of  
70 atmospheric degradation. There is no accurate understanding of the rate-controlling mechanisms,  
71 nor of the effect of glass composition and structure. What is exactly the very first step, producing  
72 the leached hydrated layer? How does the glass composition influence this step? What is the  
73 chemical and structural nature of this alteration layer? What is the rate-controlling mechanism of  
74 water diffusion through the layer and how does it depend on composition, RH and temperature?  
75 In recent years, the combined effects of RH, environment and glass composition on the very first  
76 stage of glass alteration have been studied using SIMS as high resolution chemical imaging and  
77 depth profiling technique [23–26]. These studies have highlighted the predominant role of RH in  
78 the glass surface alteration and the early mobilization of alkalis towards the surface, with a  
79 tremendous effect of the surface composition and structure on the rate of this process.

80 This study is an attempt to push forward our understanding of the mechanisms of the  
81 atmospheric alteration, which occur on a particular glass composition representative of a family  
82 of unstable historical glasses [27]. This family is characterized by, approximately, equal weight  
83 amounts of Na<sub>2</sub>O and K<sub>2</sub>O (~10% each), a moderate amount of CaO and MgO (~6%) and of  
84 Al<sub>2</sub>O<sub>3</sub> (~1%). Deciphering the mechanisms requires to measure the kinetics of the alteration  
85 process and study the changes occurring from the macroscopic to the microscopic scale. In an  
86 earlier paper [28] we reported the alteration study of this glass at 85 %RH and at 80°C, a high  
87 temperature chosen to accelerate the process. Surprising results were found, notably we did not  
88 observe the formation of a leached layer associated to alkali salts deposits on the surface. The  
89 glass surface hydration was extremely rapid. In the present paper, we describe the atmospheric  
90 alteration of the same glass at lower temperature (40°C to 60°C) and 85 %RH. The phenomena  
91 on this temperature range were markedly different, and corresponded well to the macroscopic  
92 observations reported in the literature, notably the formation of Na- and Ca-rich salts on the  
93 glass surface and the crizzling [4,5,23–26]. From the time and temperature dependency of the  
94 phenomena, and the precise compositional and structural analysis of the hydrated layers, we  
95 propose mechanisms on both temperature ranges and discuss the possible origin of the marked  
96 temperature effect.

97

## 98 2. METHODS

### 99 2.1. Sample preparation

100 Experiments were performed on one glass composition: a mixed-alkali lime silicate glass, named  
101 glass A ((wt%) SiO<sub>2</sub> 71%, Na<sub>2</sub>O 11%, K<sub>2</sub>O 11%, CaO 5%, MgO 1%, Al<sub>2</sub>O<sub>3</sub> 1%), representative  
102 of several chemically unstable productions of the Middle Ages [27]. This glass was elaborated by

103 Saint-Gobain Recherche (France) and the composition was checked by Particle Induced X-ray  
104 Emission (PIXE). Samples were prepared in the form of plates ( $1 \times 1 \times 0.3 \text{ cm}^3$ ) polished to  $1 \mu\text{m}$   
105 with aqueous suspensions of  $\text{CeO}_2$  powders. The polished plates were thoroughly cleaned before  
106 the ageing tests, using a 1M sodium dodecyl sulfate (SDS) aqueous solution and ethanol. Time of  
107 flight-secondary ion mass spectrometry (ToF-SIMS) analysis conducted on the pristine glass  
108 plates after these preparation steps showed an outermost surface layer of about 30 nm  
109 significantly depleted in Na, Ca and Mg, and slightly depleted in K (Fig. 3).

110 For bulk spectroscopy analysis, calibrated glass powders of  $32\text{-}50 \mu\text{m}$ ,  $10\text{-}20 \mu\text{m}$  and  $5\text{-}10 \mu\text{m}$  size  
111 fractions were also prepared by crushing and sieving the glass. After multiple ultrasonic washing  
112 in acetone to remove the fines, their specific surface area  $\sigma$  was measured by the BET method,  
113 using a Belsorp Max analyser with krypton as adsorbing gas. The results were  $\sigma=1200 \pm 100$   
114  $\text{cm}^2/\text{g}$ ,  $3900 \pm 300 \text{ cm}^2/\text{g}$  and  $7800 \pm 900 \text{ cm}^2/\text{g}$  for the powder fractions of  $32\text{-}50$ ,  $10\text{-}20$  and  
115  $5\text{-}10 \mu\text{m}$  respectively.

116

## 117 **2.2. Ageing tests**

118 Two different devices were used in parallel to simultaneously control the relative humidity and  
119 the temperature of the ageing atmosphere over various time periods: (i) a climatic chamber and  
120 (ii) a hermetic box put into an oven and containing a saturated saline solution to control the RH  
121 [29]. All details about these devices are given in [28]. The relative humidity was fixed at 85 RH%  
122 in all experiments and the temperature was  $40^\circ\text{C}$ ,  $50^\circ\text{C}$ ,  $60^\circ\text{C}$  or  $80^\circ\text{C}$  [28] for various periods of  
123 time from 6 h (at  $80^\circ\text{C}$ , [28]) to 9 months (at  $40^\circ\text{C}$ ). With the hermetic box, the 85%RH value  
124 was obtained thanks to a solution saturated in KCl. A MadgeTech sensor was inserted in the box  
125 to control temperature and RH during the whole experiments. We took care to avoid any liquid  
126 water run-off on the samples during the heating and cooling ramps by maintaining the RH below  
127 the dew point at every temperature. All tests were performed in static mode (no cycling). In this  
128 paper, they are noted V tests or VXh, VXd or VXm tests, where X is the total duration in hours  
129 (h), days (d) or months (m) including the ramps. The good correspondence between the two  
130 ageing methods (devices (i) or (ii)) has been checked by comparing the alteration phenomena  
131 after a 2 months ageing test at  $50^\circ\text{C}$ , 85 RH%, for this glass composition as well as for other  
132 compositions. For both ageing methods, the thickness of the alteration layer was the same ( $10$   
133  $\mu\text{m}$  for glass A) and the nature and quantities of surface salts were the same (mainly Ca-bearing  
134 carbonates for glass A).

135

## 136 **2.3. Characterization methods**

137 The glass surface and sub-surface modifications after a V test were studied at  $t_1$  (end of the V  
138 test) and over a 6 months period after  $t_1$ , because certain aged glass surfaces continued to  
139 transform under the laboratory atmosphere [28]. Sample preparation before the characterization  
140 was intentionally very limited. Notably, no rinsing nor polishing were performed, because these  
141 operations may be very harmful for the alteration layers integrity [28]. When alteration products  
142 were scattered on the surface, we preferred keeping them and taking their presence into account  
143 in the interpretation of the characterization data.

144

#### 145 Microstructural observation of the glass surface

146 The surface states of the glass plates were characterized before the V tests ( $t_0$ ) and several times  
147 after the V tests ( $t_1$  and beyond) by optical microscopy in direct or grazing light using a Keyence  
148 VHX-5000 numerical microscope with a Z500 objective. This characterization was supplemented  
149 by observations with a field-emission gun electronic microscope (FEG SEM) JEOL 7800F,  
150 preferentially in secondary electron mode at low acceleration tension (2 to 7 kV), after making the  
151 glass surface conductive with a platinum deposit about 1 nm thick. The samples were submitted  
152 to a vacuum of about 1 Pa (Pt deposit) and  $5.10^{-5}$  Pa (FEG SEM) during this characterization.

153

#### 154 Measurement of the thickness of the alteration layers

155 Alteration layer thicknesses are noted  $e_a$  in this paper. The very small ones (some tens of nm to  
156 about 200 nm) were determined from the elementary concentration profiles obtained by ToF-  
157 SIMS analysis, with a ToF-SIMS V instrument (Ion-ToF company), using a  $O_2^+$  ion beam (2 keV,  
158 about 150 nA) for in-depth abrasion, a  $Bi^+$  ion beam (25 keV, 0.3 pA) for the analysis, and an  
159 unfocused electron beam of some eV for the charge neutralization. The crater is  $200 \mu m \times 200$   
160  $\mu m$  or  $300 \mu m \times 300 \mu m$  in size and at its center the analysis zone is  $50 \mu m \times 50 \mu m$  or  $100 \mu m$   
161  $\times 100 \mu m$  respectively. The sputtering rate on aged glass plates was determined thanks to  
162 mechanical profilometry of the craters (about 0.3 nm/s into the alteration layer for a current of  
163 100 nA). To assess  $e_a$ , we considered the distance over which the  $^{45}SiOH^+/^{28}Si^+$  ratio is halfway  
164 between its near surface concentration (the value measured just after the SiOH surface spike) and  
165 its baseline concentration, as a marker of the interface between the alteration layer and the  
166 pristine glass, by analogy with a method described in [30] using the  $^1H^+/^{28}Si^+$  ratio.

167 For the high enough altered thicknesses ( $> 200$  nm), their evaluation by SEM observations was  
168 preferred. When flakes formed on glass plates, their thickness was measured and associated to  
169 the alteration layer thickness after we had checked that the flaking indeed occurred near the  
170 interface between the alteration layer and the pristine glass. Otherwise, SEM observations were  
171 performed on the edge, on a freshly fractured plate, preferentially in backscattered electron mode

172 to visualize the chemical contrast at the interface. These observations were performed in  
173 different areas of a same aged glass plate and we report a mean thickness  $e_a$ .

174

#### 175 Chemical analysis

176 Elementary compositions of the alteration layers were quantified by Energy Dispersive X-ray  
177 spectroscopy (EDX) with the system Bruker QUANTAX 400, at the same time as SEM  
178 observations. Analyses were performed either on the surface of the glass plate, outside any defect  
179 or crystal, according to the operating conditions and specific quantification method described in  
180 [28], or on the edge of the fresh fracture for the alteration layers thick enough. Elementary  
181 composition profiles into the alteration layers, from the surface to the alteration layer-pristine  
182 glass interface, were obtained by the ToF-SIMS analysis of an area free of salt deposits when  
183 possible. Chemical characterization of the alteration products on the surface of glass plates were  
184 performed by EDX at low acceleration tension, by X-Ray Diffraction (XRD) with an X'Pert  
185 PRO PANalytical instrument using Cu-K $\alpha$  radiation, and by micro-Raman spectroscopy with a  
186 Renishaw Invia instrument using a 532 nm solid-state laser as excitation light.

187

#### 188 Hydration rate measurement

189 The amount of water in the alteration layer, or hydration rate, was measured on glass plates by  
190 EDX according to the original method described in [28]. This local measurement corresponds to  
191 the water content that has not been evaporated under vacuum, i.e. to the tightly bound water. For  
192 a comparison, global weight measurements on glass powders by thermogravimetric analysis  
193 (TGA) were performed on a NETZCH STA449 F3 Jupiter equipment, considering that the  
194 tightly bound water disappears between about 150 and 500 °C [31].

195

#### 196 Structural studies

197 Structural modifications of the glass at the atomic scale were studied by the mean of solid-state  
198 Nuclear Magnetic Resonance (NMR) spectroscopy on pristine and bulk altered glass powder.  $^1\text{H}$ ,  
199  $^{23}\text{Na}$ ,  $^{27}\text{Al}$  and  $^{29}\text{Si}$  magic-angle spinning (MAS) NMR spectra were collected on Bruker Advance I  
200 and Advance II spectrometers operating at magnetic fields of 7.02 T (300WB) and 11.72 T  
201 (500WB), respectively. For these experiments, about 100 mg of a sample was packed in 4 mm  
202 outer diameter ZrO $_2$  rotor and spun from 10 kHz (7.02 T) to 12.5 kHz (11.72 T) using Bruker  
203 CPMAS probes. Recycle delay applied for the complete relaxation of nuclear magnetizations was  
204 about 1 s for  $^1\text{H}$ ,  $^{23}\text{Na}$  and  $^{27}\text{Al}$  nuclei and from 20 to 200 s for the  $^{29}\text{Si}$  nucleus.  $^1\text{H}$  spectra were  
205 acquired using the Hahn echo pulse sequence (90-  $T_E$ -180- $T_E$ -Acq) with a variable rotor-  
206 synchronized echo delay  $T_E$ .  $^1\text{H}$ - $^{29}\text{Si}$  Cross-Polarization MAS experiments (CPMAS  $^1\text{H}\rightarrow^{29}\text{Si}$ )

207 were performed with contact times of about 1 ms. Chemical shifts are referenced using a  
208 tetrakis(trimethylsilyl)silane sample for  $^1\text{H}$  (0.2 ppm relative to liquid tetramethylsilane, TMS) and  
209  $^{29}\text{Si}$  (for which the highest intensity peak is situated -9.9 ppm from that of liquid TMS), an  
210 aqueous solution of NaCl for  $^{23}\text{Na}$  (0 ppm) and an aqueous solution of  $\text{AlNO}_3$  for  $^{27}\text{Al}$  (0 ppm).  
211 In this paper, we employ the  $\text{Q}^n$  notation to describe the structure of the silicate network at short  
212 distance.  $\text{Q}^n$  represents a  $\text{SiO}_4$  unit with n bridging oxygen atoms (NBO).

213

### 214 3. RESULTS

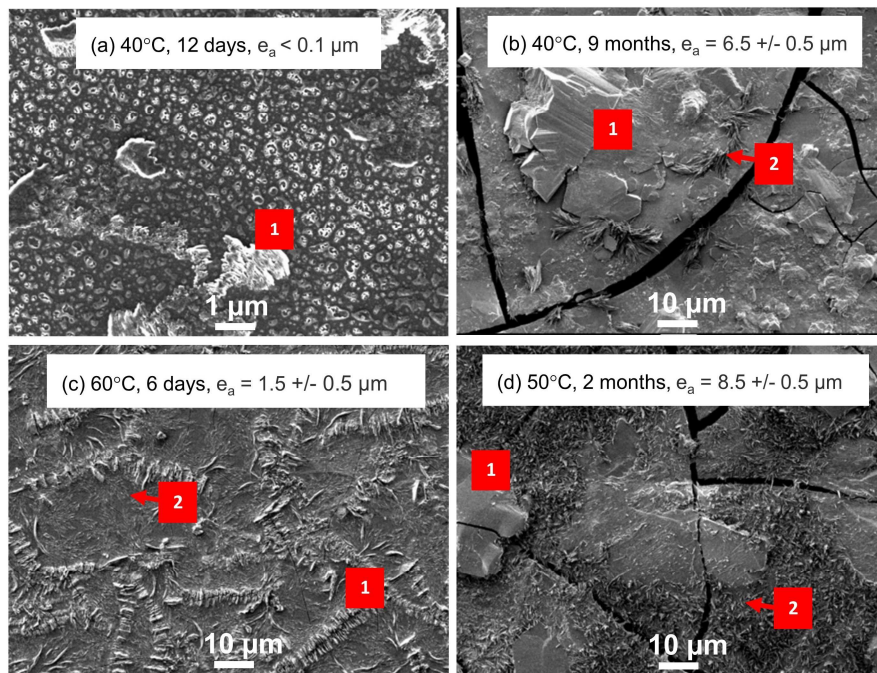
215 Contrary to the phenomena at  $80^\circ\text{C}$ , temperature at which no carbonate salts formed on the  
216 surface of the glass plates during their ageing in the climatic chamber, in the  $40\text{-}60^\circ\text{C}$  temperature  
217 range the formation and growing of the carbonate salts did occur during the ageing. After a time  
218 period depending on the temperature, the salts totally covered the surface. Below the crust of  
219 salts, a hydrated layer partially depleted in alkali and completely depleted in Ca was observed,  
220 characterized by its uniform thickness, its structural homogeneity at the SEM scale, and a flat  
221 interface to the pristine glass. When the thickness of the layer reached about  $1\ \mu\text{m}$ , the layer  
222 cracked and eventually delaminated at some locations. Except an accelerating effect of the  
223 temperature, the macroscopic phenomena were similar at  $40$ ,  $50$  and  $60^\circ\text{C}$ . The temperature of  
224  $40^\circ\text{C}$  was chosen for an in-depth study of the kinetics and chemical and structural characteristics  
225 of the alteration. After a short description of the morphological observations at  $40$ ,  $50$  and  $60^\circ\text{C}$ ,  
226 we present the results on the kinetics (as given by the alteration layer thickness as a function of  
227 time), and the detailed chemical and structural study of the alteration layer that forms at  $40^\circ\text{C}$ ,  $85$   
228 RH%. The results obtained at  $80^\circ\text{C}$ ,  $85$  RH% are given for comparison. Note that we name  
229 “alteration layer” the entire layer composed of the hydrated layer and the crust of salts on its  
230 surface.

231

#### 232 3.1. Microstructure of the alteration layers as a function of time and temperature

233 The SEM images of a selection of altered surfaces are shown in Fig. 1, and the edge of fresh  
234 fractures, or of delaminated flakes are shown in Fig. 2. Optical microscopy images, more  
235 informative about the optical macroscopic appearance of the samples, as well as complementary  
236 SEM images are given in the Data in Brief associated to this paper. The sample aged at  $40^\circ\text{C}$  for  
237 12 days provides the earliest stage of alteration in our series of experiments. Two kinds of salts  
238 have appeared at this early stage: micrometric salts with sharp angles and faces and  
239 submicrometric salts with no specific shape (Fig. 1a). From SEM-EDX and microRaman  
240 analysis, the big microscopic salts are assigned to calcite and labelled with number 1 on the

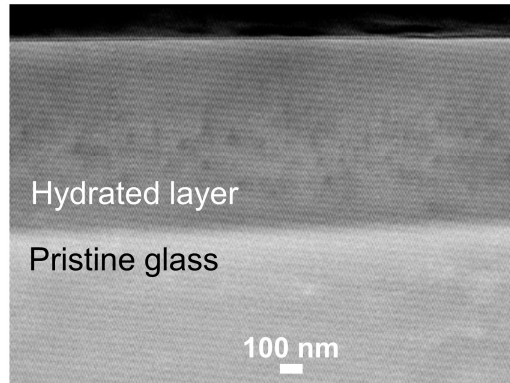
241 images. The glass surface is still visible below the salts, which appear with a shallow white  
242 boundary due to electronic charge effects. At this stage, the alteration layer thickness is less than  
243 100 nm as described later. The coverage of the surface by salts is almost complete after 3 months  
244 of ageing. At this ageing duration and beyond, scattered Na enriched carbonates with a  
245 characteristic needle-like shape sometimes referred to as “crow’s feet”[14] are observed and  
246 identified by EDX (Na and C enrichment). These salts are labelled with number 2 in Fig. 1b, c  
247 and d. Immediately next to the calcite crystals, other small and shapeless precipitates enriched in  
248 Ca, C and O are also observed (Data in Brief Fig. 1d, label 3) and assigned to vaterite. After 9  
249 months of ageing at 40°C, the longest experimental period of the study, the salts form a  
250 continuous crust on the top of the glass hydrated layer, which is about 6.5 µm thick (Fig. 2b).  
251 The calcite is always recognizable as distinctive crystal stacks with large faces (Fig. 1b, label 1), as  
252 are the needle-like Na enriched carbonates (Fig. 1b, label 2). Due to the insufficient amount of  
253 salts, only the calcite phase was identified by XRD. The microRaman spectrum of a glass powder  
254 (6-10 µm) altered for 6 months at 40°C, bears the distinctive peaks of calcite (283, 715 and 1087  
255 cm<sup>-1</sup>) and an additional peak at 1071 cm<sup>-1</sup> that could indicate the presence of pirssonite, a mixed  
256 soda-lime carbonate of composition Na<sub>2</sub>Ca(CO<sub>3</sub>)<sub>2</sub>·2H<sub>2</sub>O (RRUFF database, reference R040146).  
257 At 40°C, the cracking of the hydrated layer starts after 3 months of ageing, when the hydrated  
258 layer is 1±0.2 µm thick. The cracks cut across the salts (see for instance Fig. 1d, the calcite crystal  
259 on the left). It means that they have occurred after the formation of the salts, possibly during the  
260 ramp to ambient temperature and RH, because of stresses induced by differential dilatation and  
261 loss of water. The delamination, which opens an air gap below the flakes, is well put in evidence  
262 by the observation of circular interference patterns by optical microscopy (Newton rings) (Data  
263 in Brief Fig. 1b). It begins after 6 months of ageing (hydrated layer thickness is 2.5±0.2 µm).  
264 Flakes are about 100 µm in length, a size that seems independent of the temperature and time  
265 (compare Fig. 1b and d).



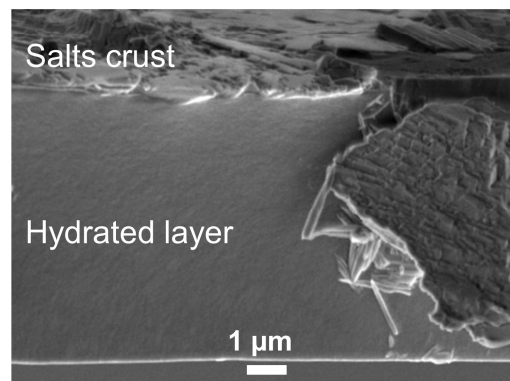
266  
 267 **Fig. 1** Surface states of glass A plates immediately after an ageing ( $t_1$  time) at 40 °C (a,b), 60 °C  
 268 (c) or 50 °C (d), 85 RH%. Secondary electrons SEM images.  $e_a$ : alteration layer thickness. Label 1  
 269 depicts calcite crystals and label 2 sodium-bearing carbonate crystals.

270  
 271 At 50°C and 60°C, the morphology is comparable but the alteration is more rapid. After 2  
 272 months of ageing at 50°C, the alteration layer is composed of an irregular crust of carbonates of  
 273 thickness up to about 2 μm, and underneath, of a hydrated layer about 8.5 μm thick (Fig. 1d and  
 274 Fig. 2c). At 60°C and 6 days of ageing, the carbonate salts almost cover the surface, the hydrated  
 275 layer underneath is already 1.5 μm thick and crossed by cracks (Fig. 1c). Vaterite crystals ( $\text{CaCO}_3$ )  
 276 were identified (DRX, Raman) together with calcite crystals ( $\text{CaCO}_3$ ). The morphology of the  
 277 calcite crystals is different than at lower temperature: small calcite crystal plates perpendicular to  
 278 the surface are stacked as chains of several 10 μm length. This microstructure characterized by  
 279 more numerous and smaller crystals is likely related to a higher nucleating rate of calcite at this  
 280 temperature. The visual appearance of this sample was completely opaque and white.

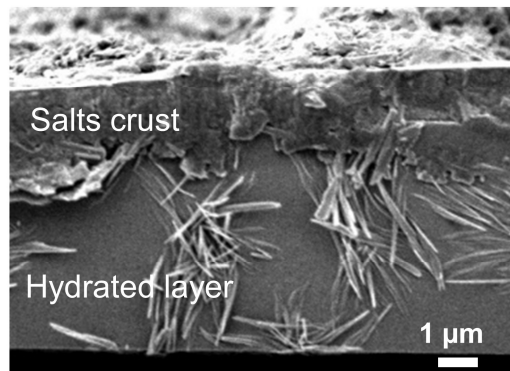
281



(a) 40°C, 3 months,  $e_a = 1 \pm 0.2 \mu\text{m}$



(b) 40°C, 9 months,  $e_a = 6.5 \pm 0.5 \mu\text{m}$



(c) 50°C, 2 months,  $e_a = 8.5 \pm 0.5 \mu\text{m}$

282

283 **Fig. 2** SEM images of the edge of glass A plates after an ageing at 40 °C (a,b) or 50°C (c), 85  
 284 RH%. Secondary electron mode (b, c) or backscattered electron mode (a).  $e_a$ : alteration layer  
 285 thickness.

286

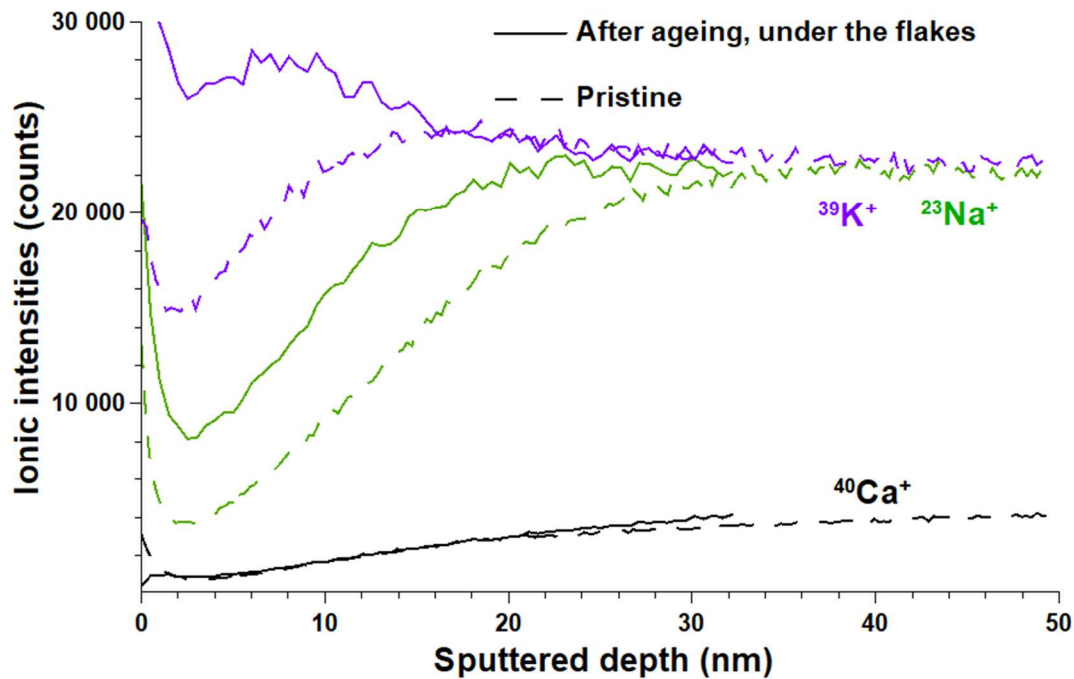
### 287 3.2. Growing kinetics of the alteration layer

288 As described above, the atmospheric alteration in the 40-60°C temperature range manifests by  
 289 the concomitant formation of a hydrated layer and of carbonate salts on the top of it. At 80°C,  
 290 only the formation of the hydration layer is observed during the ageing. Carbonate salts form

291 after the end of the ageing test, when samples have cooled down to ambient temperature and RH  
292 [28]. Interestingly, calcite is never observed on these 80°C aged samples, but only Na carbonates,  
293 among which trona only could be identified (a hydroxycarbonate with composition  
294  $\text{Na}_3(\text{HCO}_3)(\text{CO}_3)\cdot 2\text{H}_2\text{O}$ ) [28]. Whatever the ageing duration and temperature (40, 50, 60 and  
295 80°C), the hydrated layer has always the same microscopic characteristics: it has a uniform  
296 thickness, delimited by a flat and sharp interface with the pristine glass at the SEM scale (about  
297 0.1  $\mu\text{m}$ , Fig. 2a). The dark contrast with the pristine glass is due to partial loss of alkali and lime  
298 and hydration (see later), but also probably to a reduced density. The granularity observed at very  
299 small scale on the SEM images of the edge is of topological nature (by comparing secondary and  
300 back-scattered electrons images). It probably reflects structural inhomogeneity at the nanometer  
301 scale. At last, the flatness of the alteration layer-pristine glass interface again demonstrates that  
302 the cracking probably occurred during the ramp of temperature and RH at the end of the ageing,  
303 otherwise irregularities of the interface around the cracks would be expected.

304 After the layer has reached one micrometer thickness (1  $\mu\text{m}$ ), it cracks and eventually forms  
305 delaminated flakes. The concentration profile of the glass beneath the detached flakes was  
306 measured by ToF-SIMS for the sample altered at 50°C for 2 months. It is compared with the  
307 profile of the pristine, polished glass plates in Fig. 3 (only ionic intensities of  $^{39}\text{K}^+$ ,  $^{23}\text{Na}^+$  and  
308  $^{40}\text{Ca}^+$  are depicted). The surface of the pristine glass is depleted in Na and K over about 30 nm,  
309 due to the polishing by  $\text{CeO}_2$  powder in water. The surface of the glass below the detached flakes  
310 is less depleted in Na in comparison, and not depleted in K. On the contrary, there is a slight K-  
311 enrichment over the first 20 nm below the surface. It means that the delamination occurs within  
312 20 nm of the hydration front. A local K-enrichment around the hydration front has been  
313 reported in another study of glass alteration in silica-saturated solution [32]. From this result, it  
314 can be considered that the thickness of the flakes corresponds to the thickness of the hydrated  
315 layer. The conclusion was the same at 80°C, because the EDX analysis of the glass below the  
316 flakes was identical to that of the pristine glass (Table 4 in [28]).

317



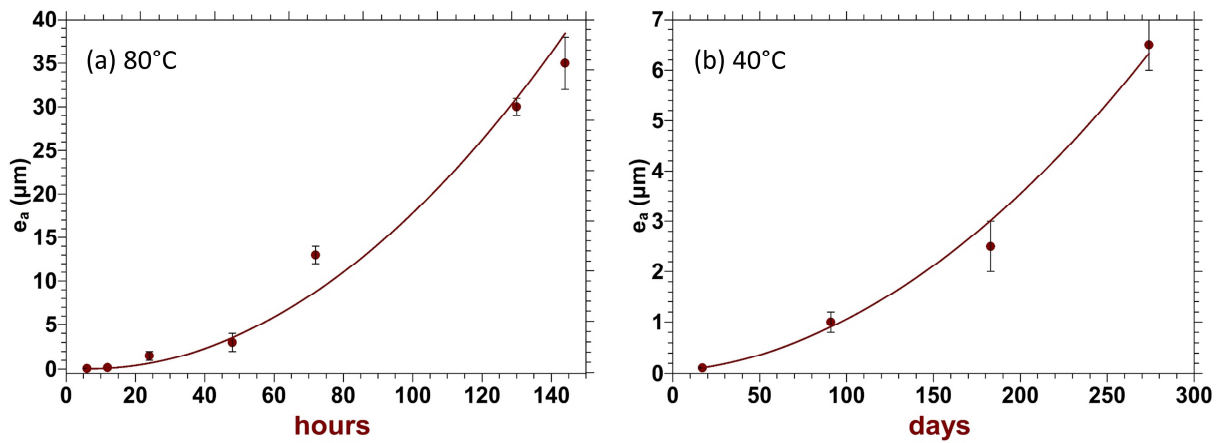
318  
 319 **Fig. 3** Ionic intensities in  $^{39}\text{K}^+$ ,  $^{23}\text{Na}^+$  and  $^{40}\text{Ca}^{2+}$  measured by TOF-SIMS on a pristine glass plate  
 320 after polishing and washing (dashed curve) and on the glass surface below the flakes of a glass  
 321 plate aged at  $50^\circ\text{C}$  and 85 %RH for 2 months (continuous curve).  
 322

323 The hydrated layer thickness was then measured by ToF-SIMS profiling at short ageing time (6h,  
 324 12h at  $80^\circ\text{C}$  and 17 days at  $40^\circ\text{C}$ ), and by SEM at longer ageing time. Values are given in Table 1  
 325 and plotted as a function of time in Fig. 4.

326 In the timescale of the experiments, the growing of the hydration layer tends to accelerate at  
 327  $80^\circ\text{C}$  and at  $40^\circ\text{C}$ . Surprisingly, the hydration kinetics is neither at the square-root of time nor  
 328 linear, indicating that it is neither simply diffusion controlled nor surface-controlled. Several  
 329 mechanisms interplay to explain this acceleration that will be discussed later. A complex time  
 330 dependency has also been found at room temperature for soda-lime silicate glasses, although the  
 331 very short alteration depths hinders accurate measurement of the kinetics [26].

332 Moreover, we emphasize that the time and  $e_a$  scales are very different in Fig. 4a ( $80^\circ\text{C}$ ) and Fig.  
 333 4b ( $40^\circ\text{C}$ ). By neglecting the acceleration and assuming a linear rate, the alteration layer thickness  
 334 increases by approximately  $6\ \mu\text{m}/\text{day}$  at  $80^\circ\text{C}$  and by about  $24\ \text{nm}/\text{day}$  at  $40^\circ\text{C}$ , which would  
 335 correspond to a very high apparent activation energy of about  $130\ \text{kJ}/\text{mol}$ . Such a value far  
 336 exceeds the activation energy reported for silicate network hydrolysis (about  $80\text{-}85\ \text{kJ}\cdot\text{mol}^{-1}$  for  
 337 silicate glasses [33,34]). This result suggests that i) either the rate-controlling mechanisms are  
 338 different at  $80^\circ\text{C}$  and at  $40^\circ\text{C}$ , or ii) the rate-controlling mechanisms are the same but their

339 kinetics parameters (activation energy, prefactor) have changed with the temperature.



340  
 341 **Fig. 4** Alteration layer thicknesses ( $e_a$ ) of glass A as a function of the ageing duration (numerical  
 342 values are reported in Table 1). The lines are a guide for the eyes. (a) 80 °C, 85 RH% (climatic  
 343 oven). (b) 40 °C, 85 RH% (V17d: climatic oven, other ageing durations: hermetic box containing  
 344 a saline solution of KCl in H<sub>2</sub>O).

345

80 °C							
	6 h	12 h	24 h	48 h	72 h	130 h	144 h
$e_a$ (µm)	0.055 ± 0.01 *	0.07 ± 0.01 *	1.5 ± 0.5	3 ± 1	13 ± 1	30 ± 3	35 ± 3
40 °C							
	17 d	3 m	6 m	9 m			
$e_a$ (µm)	0.11 ± 0.01 *	1 ± 0.2	2.5 ± 0.2	6.5 ± 0.5			

346 **Table 1.** Alteration layer thicknesses ( $e_a$ ) of glass A developed with various ageing durations at 80  
 347 °C (climatic oven) or at 40 °C (V17d: climatic oven, other ageing durations: hermetic box  
 348 containing a saline solution of KCl in H<sub>2</sub>O), 85 %RH, as determined by SEM observations or (\*)  
 349 from ToF-SIMS profiles.

350

### 351 3.3. Composition of the alteration layer

352 The composition of the alteration layer has been measured by EDX with an acceleration tension  
 353 of 7 kV, on the surface, in an area free of carbonate salts, for the samples aged for 3 months or 6  
 354 months at 40°C. At this tension, the analyzed depth is equal to, or less than, 0.6 µm for all the  
 355 elements of the glass (calculation with the STRATAGEM software). Therefore, the alteration  
 356 layer only contributes to the chemical analysis. The glass plate aged for 9 months at 40°C has  
 357 developed an alteration layer of 6.5 µm in thickness, which has started to delaminate. It was thus  
 358 possible to measure the composition on the edge, by scanning a 1 µm<sup>2</sup> area at two distinct

359 locations: near the surface (location 1) and near the interface with the pristine glass (location 2).  
 360 For the different analyses, the mass elemental fractions totaled 92.5% to 95%. The difference is  
 361 attributed to the contribution of protons and to porosity (because the contribution of protons is  
 362 of the order of 1 wt% according to the estimated H<sub>2</sub>O content, see below). The elemental  
 363 fractions reported in Table 2 are normalized to 100% and compared with the composition of the  
 364 pristine glass A. The elemental ratio Na/Si, K/Si and Ca/Si and the O weight fraction calculated  
 365 from the cationic composition are also given in Table 2. The difference between the measured O  
 366 and the calculated O is attributed to water, it allows the calculation of a hydration rate given in  
 367 the last column. Note that because we used the pristine glass A as a standard for these analyses,  
 368 the error is minimized and estimated to ~1% for the major elements.  
 369

	O	Na	Mg	Al	Si	K	Ca	calculated O	Na/Si	K/Si	Ca/Si	H <sub>2</sub> O* wt%
A pristine	59.5	7.58	0.42	0.33	25.2	4.98	1.90	59.5	0.30	0.20	0.075	-
A V3m surface	63.5	5.29	0.58	0.31	25.2	4.95	0.13	56.7	0.21	0.20	0.005	6
A V6m surface	64.4	5.87	0.63	0.29	23.6	5.06	0.11	58.3	0.25	0.21	0.004	9
A V9m edge, 1	64.0	4.72	0.37	0.34	25.6	4.95	0.00	57.0	0.18	0.19	0.00	6.1
A V9m edge, 2	63.73	4.71	0.27	0.42	25.76	5.12	0.00	57.32	0.18	0.20	0.00	5.6

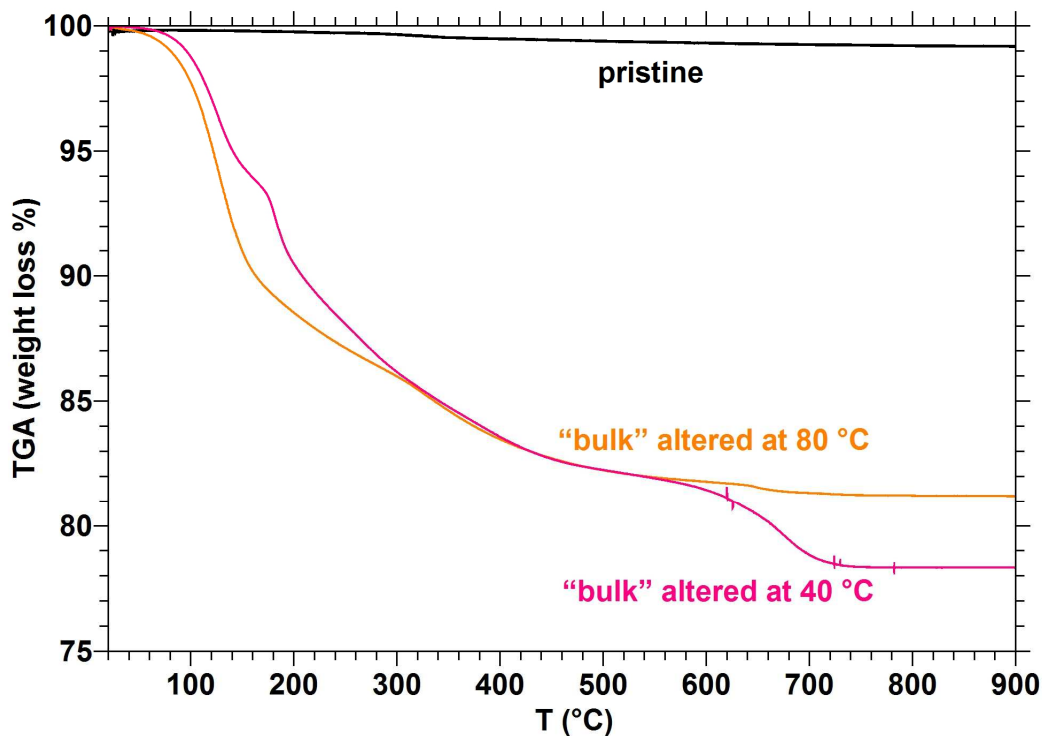
370 **Table 2.** EDX average composition (atom% element with 100% normalization) of the alteration  
 371 layers of glass A analyzed at the surface or the edge of the glass plates (7 kV acceleration tension)  
 372 after a V test at 40 °C, 85 RH%, for various ageing duration (hermetic box containing a saline  
 373 solution of KCl in H<sub>2</sub>O). Pristine glass A is used as standard and matrix effects are considered by  
 374 using the data processing software STRATAGem. \* Average hydration rate in weight %  
 375 estimated from the comparison between the oxygen atomic fraction obtained by EDX and the  
 376 one calculated by stoichiometry (calculated O column). Concentration ratios R/Si (R=Na, K, Ca)  
 377 are calculated from EDX results.

378  
 379 These chemical analyses indicate that the hydrated layer is partially depleted in Na (about 40% of  
 380 the Na is lost after 9 months), and totally depleted in Ca. It is not depleted in K. Concerning Mg,  
 381 it is still present in the layer but as a minor element, its analysis is not accurate enough to

382 comment the variation. Its presence could not be put in evidence in the carbonate precipitates on  
383 the surface.

384 The hydration rate of the layer is 6 to 9 wt%. It can be compared to the hydration rate estimated  
385 by thermogravimetric analysis of bulk altered glass powder. According to the thickness of the  
386 alteration layer after 6 months of ageing (2.5  $\mu\text{m}$ ), the 5-10  $\mu\text{m}$  powder fraction aged for 6  
387 months should be altered in the bulk and this has been verified by  $^{27}\text{Al}$  and  $^{23}\text{Na}$  MAS NMR.  
388 Three thermograms are shown in Fig. 5: the 5-10  $\mu\text{m}$  powder aged for 6 months at 40°C, the 32-  
389 50  $\mu\text{m}$  powder aged for 72h at 80°C [28] and a pristine glass A powder. The mass loss below 150-  
390 200°C is attributed to weakly bound molecular water, it is around 10 wt% at both 80°C and 40°C  
391 (the kink on the 40°C powder thermogram is possibly due to the dehydration of  
392 hydroxycarbonates). We observed that the mass loss in this temperature range depends on the  
393 conservation conditions of the powders (inside or outside a dessicator for instance), indicating an  
394 equilibrium of this weakly bound water with the atmosphere (RH). This water is lost when the  
395 samples are put under vacuum in the SEM chamber, so that the mass loss that should be  
396 compared with the SEM hydration rate is that measured beyond 150-200°C. On this temperature  
397 range, there is a mass loss event between 600 and 700°C in the 40°C altered glass powder, which  
398 corresponds to the decomposition of carbonates ( $\text{CO}_2$  departure). This event is minimized in the  
399 80°C altered powder because no carbonates formed at this temperature as described before (a  
400 few carbonates appeared after the ageing). The hydration rate evaluated by the mass loss in the  
401 150-500°C range, taking into account the contribution of carbonates to the total mass of the  
402 40°C altered powder, is about 8 wt%, in very good agreement with the EDX hydration rate  
403 (Table 2). The hydration rate of the 80°C altered powder is similar. The mass of  $\text{CO}_2$  in the  
404 carbonates is 4.4 wt% of the mass of the 40°C altered powder. It is consistent with the calculated  
405 mass of  $\text{CO}_2$  in calcite by assuming that all the Ca in this altered glass powder has formed calcite  
406 (3.9 wt%), the difference being assigned to the presence of Na-bearing carbonates. This  
407 consistency between glass plates data and glass powder data is important to emphasize because it  
408 gives robustness to our structural study based on the analysis of altered glass powders.

409



410 **Fig. 5** Thermogravimetric analysis of pristine glass A powder and “bulk” altered glass A powders  
 411 after an ageing at 80 °C (32-50  $\mu\text{m}$ , V72h, climatic oven) or at 40 °C (5-10  $\mu\text{m}$ , V6m, hermetic  
 412 box containing a saline solution of KCl in  $\text{H}_2\text{O}$ ), 85 %RH. Bulk alteration was checked by  $^{27}\text{Al}$   
 413 MAS NMR.

414  
 415 By comparing the EDX analysis at the top of the hydrated layer (Table 2, 9 months, location 1)  
 416 or at the bottom (Table 2, 9 months, location 2), we notice that the hydrated layer is chemically  
 417 homogeneous. The absence of chemical gradients points out the fact that all the water-glass  
 418 reactivity occurs at the interface (within 0.1  $\mu\text{m}$  that is our SEM-EDX spatial resolution), leaving  
 419 behind a hydrated layer that is apparently at equilibrium with the atmosphere and the carbonate  
 420 salts on the surface. Nevertheless, this equilibrium is only apparent because the Na content of the  
 421 hydrated layer slowly decreases as a function of the ageing time (compare 3 months and 9  
 422 months in Table 2). Another remarkable feature is the complete absence of K depletion,  
 423 consistent with the absence of K in the carbonate precipitates. There is a striking contrast  
 424 between the behavior of K (not at all depleted) and Ca (totally depleted).

425 An attempt to examine the interface between the hydrated layer and the pristine glass has been  
 426 carried out by TOF-SIMS profile analysis of glass plates aged at 40°C for 17 days and for 3  
 427 months. Because of the presence of carbonates on the surface, this attempt was not successful in

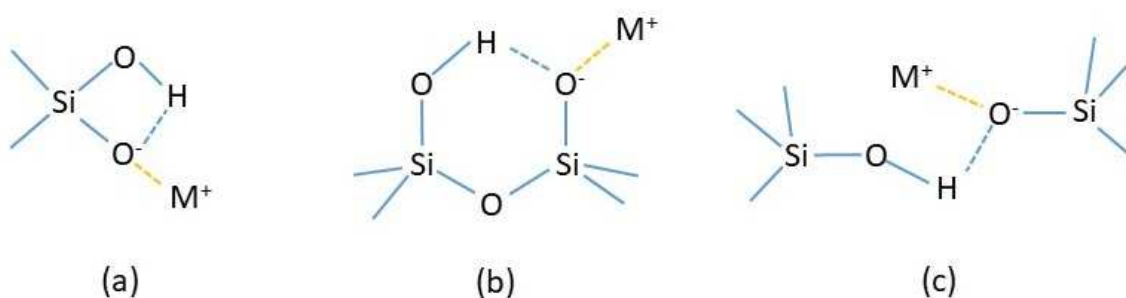
428 accurately profiling the interface, but it confirmed the extent of the depletion of the various  
429 cationic elements. The description of this result is placed in the Data in Brief associated to this  
430 paper.

431

#### 432 3.4. Atomic structure of the alteration layer

433 Glass powders of 5-10  $\mu\text{m}$ , 10-20  $\mu\text{m}$  and 32-50  $\mu\text{m}$  have been aged for 6 months at 40°C, or 2  
434 months at 50°C, or 12 days at 60°C (85 %RH) respectively, in order to produce alteration in the  
435 bulk. The spectra of the bulk altered glass powder (32-50  $\mu\text{m}$ ) aged at 80°C published in [28] are  
436 reported also for comparison. The  $^1\text{H}$  MAS NMR spectra at the different temperatures are  
437 compared in Fig. 6a while the Hahn echo (HE) acquisitions of the 40°C altered powder are  
438 shown as a function of varying echo time  $T_E$  in Fig. 6b (peaks of the species experiencing the  
439 strongest homonuclear  $^1\text{H}$ - $^1\text{H}$  dipolar interactions – thus in a dense proton network – decrease  
440 faster; thus using a variable echo delay helps identify different environments). These series of HE  
441 spectra put in evidence at least 5 hydrated species in the aged glass: a broad signal at about +5  
442 ppm, two high frequency signals at +10 ppm and +14 ppm and two weak, narrow signals at  
443 about 0-+3 ppm. The broad signal centered at +5 ppm dominates in the spinning sidebands  
444 manifold, and its relative intensity decreases rapidly with increasing  $T_E$ . Following the literature  
445 [35,36], this behavior allows to assign it to molecular water, because the strong homonuclear  
446 dipolar coupling in  $\text{H}_2\text{O}$  associated to its high concentration induce shorter spin-spin relaxation  
447 time ( $T_2$ ) and irreversible loss of this signal in the central band of the HE spectra at high echo  
448 time, with respect to the other hydrated species with weaker homonuclear dipolar coupling.  
449 Moreover, the relative intensity of this signal decreases faster in the spinning sidebands than in  
450 the central band (this is particularly visible in the  $T_E=120 \mu\text{s}$  spectrum in Fig. 6b). It means that  
451 molecular water does not account for all the intensity at about 5 ppm. Note that because of these  
452 irreversible losses that depend on the hydrated species (different  $T_2$  values), it is not really  
453 possible to quantify the proportion of these species by simulating the central band intensity.  
454 Besides, the widths of these spectra have two main origins: i) the distribution of isotropic  
455 chemical shifts (inhomogeneous width) and ii) the residual homogeneous width due to the  
456 incomplete averaging (i.e., cancellation) of the dipolar couplings by the MAS. It is highly probable  
457 that in our glasses, using a MAS spinning frequency of 10 kHz, the inhomogeneous width  
458 dominates, as it has been demonstrated in hydrous aluminosilicate glasses [37].  
459 By increasing the echo time, the water signal is filtered and the other contributions with longer  $T_2$   
460 appear. The two peaks at +10 ppm and +14 ppm most likely belong to the same broad and  
461 asymmetrical distribution of intensity between +14 and +3 ppm, with most of the intensity on

462 the intermediate to high frequency side. This broad component corresponds to OH groups with  
 463 a distribution of hydrogen bonding strength. Indeed, a correlation between the chemical shift and  
 464 the O-H...O distance, which measures the strength of the hydrogen bonding, has been reported  
 465 for long in the literature and supported by theoretical calculations [35,37]. The O-H...O  
 466 distances that give account of the +10 and +14 ppm chemical shifts are 2.65 Å and 2.50 Å  
 467 respectively. Such high <sup>1</sup>H isotropic chemical shifts revealing very strong hydrogen bonding of  
 468 the OH groups are commonly observed in alkali silicate crystal hydrates [35,38,39] and in  
 469 hydrous alkali silicate glasses [40–42]. They are not observed in hydrous silica [43], nor in glasses  
 470 altered by immersion in liquid water, which are depleted in alkalis and of which <sup>1</sup>H isotropic  
 471 chemical shifts do not exceed 8 ppm [44]. Therefore, they are related to the presence of alkalis  
 472 and non-bridging oxygens (NBO) and indicate hydrogen bonding between a Si-OH group and a  
 473 Si-O(M<sup>+</sup>) group possibly connected to the same Si [38,45] with M<sup>+</sup> being an alkali, as in the  
 474 following picture where (a) is an intratetrahedral H-bonding in a hydrated Q<sup>2</sup> species, (b) is a H-  
 475 bonding between neighboring tetrahedra and (c) is a H-bonding between adjacent, but not  
 476 neighboring tetrahedra:



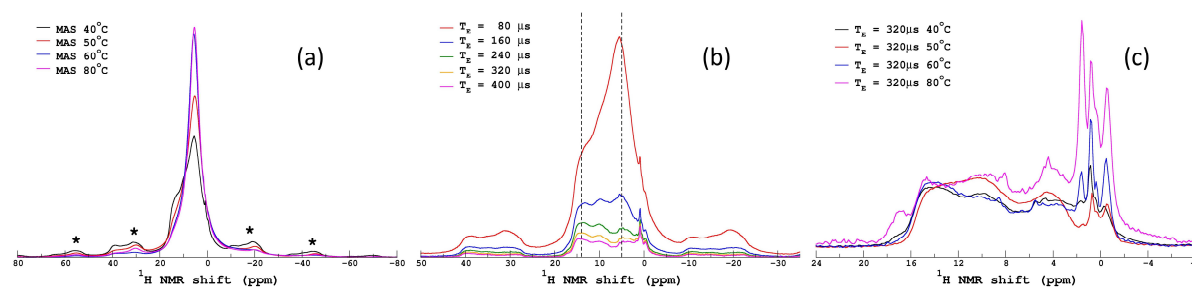
477  
 478 In the cases (b) and (c), the two tetrahedra are noted Q<sup>3</sup>-H and Q<sup>3</sup>-M,H to refer to the H-bond  
 479 of this species. The O(H)-O- distance is expected to be about 2.64 Å in the intratetrahedral H-  
 480 bonding (a), between 2.55 Å and 2.75 Å in H-bonding between neighboring tetrahedra  
 481 depending on the nature of the alkali, in the order K<Na<Li (b) [40], and distributed in (c). Note  
 482 that in these structural arrangements, the protons are almost structurally equivalent to modifier  
 483 cations. Such a proton species exists in KHSi<sub>2</sub>O<sub>5</sub> crystal structure (with  $\delta_{iso} = 15.6$  ppm) and it  
 484 has been proposed that similar NaHSi<sub>2</sub>O<sub>5</sub> units exist in sodium silicate crystal hydrates like  
 485 sodium disilicate hydrates (<sup>1</sup>H  $\delta_{iso} = 15.3$  and 18.7 ppm, [38]) and hydrates with high silica  
 486 content (octosilicate, <sup>1</sup>H  $\delta_{iso} = 16$  ppm, magadiite, <sup>1</sup>H  $\delta_{iso} = 14.9$  ppm and kenyaite, <sup>1</sup>H  $\delta_{iso} =$   
 487 15 ppm, [40]) with the difference that Na<sup>+</sup> ions are also surrounded by water molecules. In these  
 488 hydrates, by examining the <sup>1</sup>H NMR line widths and the <sup>2</sup>H (D) quadrupolar parameters of OD  
 489 groups in deuterated samples, the protons of the H-bonded OH may be considered as rigid with  
 490 respect to the NMR time scale, and they do not exchange with protons of water molecules

491 [39,45].

492 At last, narrow, weak signals at low chemical shift (0-+3 ppm) are assigned to isolated OH  
493 groups, because of their weak H-H dipolar coupling and low chemical shift. These species may  
494 be isolated Si-OH or M-OH groups, possibly in crystalline environments [35,40].

495 The comparison of the MAS spectra in Fig. 6a indicates that the relative proportion of molecular  
496 water and OH groups vary with the temperature of ageing in a regular way, with more molecular  
497 water at high temperature. The total amount of water (H<sub>2</sub>O+OH) has not been measured in  
498 these powders at the time of the NMR experiment, so that it is difficult to draw any conclusion  
499 from this tendency. As we have noticed with the TGA measurements, there is an equilibrium  
500 between the weakly bound molecular water in the layer and the atmospheric humidity. All the  
501 spectra have been measured in the same atmosphere. Either the alteration layer produced at high  
502 temperature (60°C, 80°C) takes more molecular water, or the relative proportion of the species  
503 differ: the answer needs a careful study with control of the total H<sub>2</sub>O content.

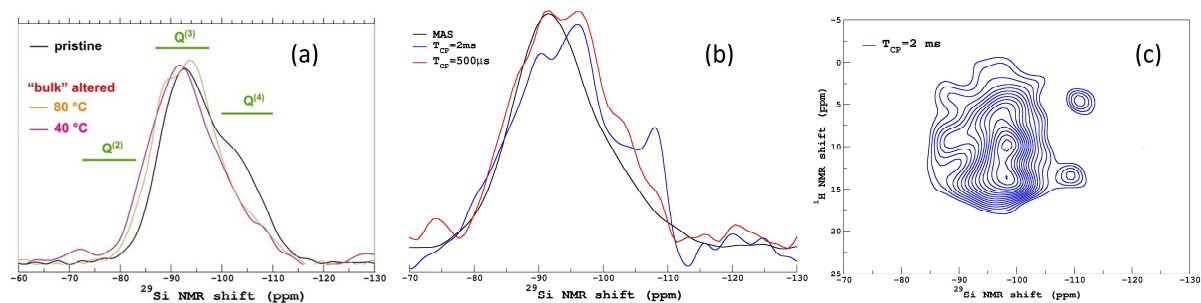
504 The HE acquisitions ( $T_E = 320 \mu s$ ) of the glass powders aged at the different temperatures are  
505 given in Fig. 6c, to compare the spectra after filtering the water (and Si-OH species close to this  
506 water having the shortest  $T_2$ ). These spectra are very similar regarding the number, positions and  
507 relative intensities of the peaks. This points out a structural similarity of the hydrated layer  
508 produced in the 40°C-80°C temperature range. The quantitative analysis of the Si-OH and water  
509 speciation would require a deeper experimental study.



510 **Fig. 6** (a) <sup>1</sup>H MAS NMR spectra of bulk altered glass A powders after an ageing at 40°C, 50°C,  
511 60°C, 80°C and 85 %RH. The spectra are normalized to the same area including the spinning  
512 side bands. \*: spinnnig sidebands. (b) Hahn echo acquisitions with variable echo delays  $T_E$  of the  
513 bulk altered powder produced at 40°C, 85 RH%. (c) Hahn echo acquisitions ( $T_E = 320 \mu s$ ) of the  
514 bulk altered glass A powders produced at the different temperatures. The spectra are normalized  
515 in height to the peak intensity centered around +14 ppm.

516  
517  
518 The <sup>29</sup>Si MAS NMR spectra of the pristine and altered glass A at 40°C and 80°C are depicted in  
519 Fig. 7a. Intermediate temperatures give similar spectra and are therefore not shown. The

520 simulation of the pristine glass spectrum gives 35% of  $Q^4$  species at -103 ppm and 65% of  $Q^3$   
521 species at -92 ppm, in excellent agreement with the glass A composition assuming homogeneous  
522 distribution of the NBOs in the silicate network, and with the chemical shifts in the literature  
523 [46]. After ageing in humid atmosphere at both temperatures, the  $Q^4$  band decreases very  
524 significantly while the  $Q^3$  band maintains its intensity and is enlarged on the high frequency-side.  
525 The apparition of a few  $Q^2$  units might explain part of this enlargement, but the main part is  
526 probably owed to the widening of the  $Q^3$  chemical shift distribution because of a greater variety  
527 of  $Q^3$  species ( $Q^3$ -H and  $Q^3$ -Na and all the intermediate  $Q^3$ -H,Na species with varying H-  
528 bonding strength). We notice that there is a double-peak in the  $Q^3$  component of the glass  
529 powder aged at 80°C, which is not visible in the powder aged at 40°C. This double-peak appears  
530 in the  $^1\text{H} \rightarrow ^{29}\text{Si}$  CP MAS spectrum of this latter powder, with a long contact time (2 ms, Fig.  
531 7b). Indeed, although no efficient  $^1\text{H} \rightarrow ^{29}\text{Si}$  cross-polarization could be achieved on the 80°C  
532 altered powder (possibly because of a high amount of short  $T_2$  H species), it was possible to  
533 acquire  $^1\text{H} \rightarrow ^{29}\text{Si}$  CP MAS and HETCOR spectra on the 40°C altered powder, shown in Fig. 7b  
534 and 7c. At short contact time (0.5 ms), all the hydrated species are in the vicinity of a wide  
535 distribution of  $Q^3$  (and possibly  $Q^2$ ) units. However, at long contact time (2 ms), two additional  
536  $Q^n$  species show up at a longer distance to protons: a  $Q^4$  signal at about -109 ppm, remarkably  
537 narrow, and a  $Q^3$  signal at about -96 ppm analogous to the low-frequency peak in the 80°C  
538 altered powder. Thus, we propose to assign the  $Q^3$  low-frequency peak (-96 ppm) to  $Q^3$ -Na  
539 species, or to  $Q^3$ -Na,H species undergoing weak H-bonding (long O---H distance), and the high-  
540 frequency peak (-88 ppm) to  $Q^3$ -H species, or to  $Q^3$ -Na,H species undergoing strong H-bonding  
541 (short O---H distance). This assignment is consistent with the fact that  $Q^3$ -Na species are  
542 expected to be more abundant in the 80°C altered glass, because it has retained all the alkali [28]  
543 with respect to the 40°C altered glass that has lost up to 40% of the alkalis. On the other hand,  
544 the narrow  $Q^4$  signal is not expected in a glass. Its  $^{29}\text{Si}$  chemical shift is the same as in cristobalite  
545 [47]. This suggests the possible presence of locally ordered re-polymerized areas in the hydrated  
546 glass at 40°C, in agreement with hints of a re-polymerized component in the corresponding  
547 Raman spectra (see below).  
548



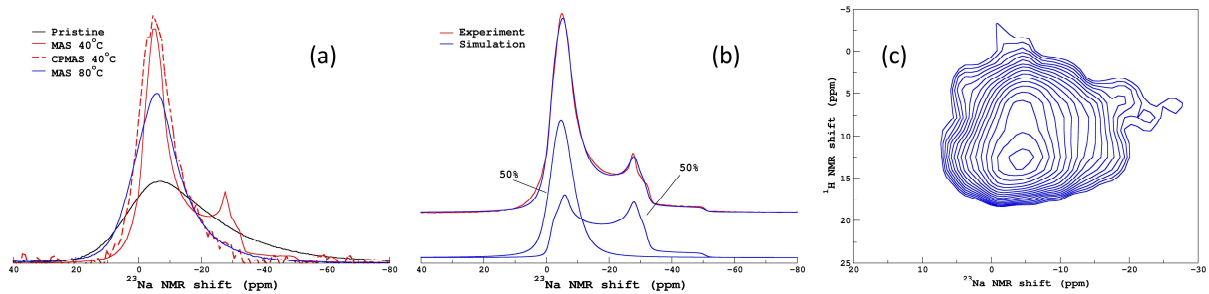
549  
 550 **Fig. 7** (a)  $^{29}\text{Si}$  MAS NMR spectra of bulk altered glass A powders after an ageing at 40°C or 80  
 551 °C, 85 %RH. The  $^{29}\text{Si}$  NMR MAS spectrum of pristine glass A powder is reported for reference.  
 552 (b) CPMAS  $^1\text{H}$ - $^{29}\text{Si}$  acquisition for two contact times ( $T_{\text{CP}}$ ) of the bulk altered glass A powder  
 553 aged at 40°C, 85 RH% and (c) HETCOR  $^1\text{H}$ - $^{29}\text{Si}$  acquisition of the same powder for  $T_{\text{CP}}=2$  ms.

554  
 555 This NMR study has been completed by  $^{23}\text{Na}$  MAS NMR and  $^1\text{H} \rightarrow ^{23}\text{Na}$  CP experiments on the  
 556 altered powders, reported in Fig. 8. The  $^{23}\text{Na}$  MAS NMR spectrum of the pristine glass A shows  
 557 a broad asymmetrical profile which is typical of Na in alkali silicate glasses [48,49]. The  
 558 broadening originates from the distribution of both the isotropic chemical shift and the second-  
 559 order quadrupolar interaction. These spectra have been fitted following the procedure described  
 560 in [50]. The fit of the 40°C altered powder is shown in Fig. 8b and the fit parameters are reported  
 561 in Table 3.

562 Comparing the pristine glass A and the glass powder aged at 80°C, the  $^{23}\text{Na}$  NMR parameters  
 563 indicate a very slight increase of the Na-O mean distance, and an environment that has become  
 564 more centrosymmetrical with the alteration (see discussion in [28]). The  $^{23}\text{Na}$  NMR spectrum of  
 565 the glass powder aged at 40°C bears two signals, the signal of  $\text{Na}^+$  in the hydrated glass, having a  
 566  $^{23}\text{Na} \delta_{\text{iso}} \sim -2.7$  (2.3) ppm and  $C_Q \sim 1.1$  (0.5) MHz (standard deviation under brackets) and the  
 567 sharp signal of  $\text{Na}^+$  in a crystalline phase that may possibly be assigned to Na, Ca mixed hydrated  
 568 carbonates such as gaylussite ( $\text{Na}_2\text{Ca}(\text{CO}_3)_2 \cdot 5\text{H}_2\text{O}$ ) that has been identified on the Raman  
 569 spectrum (Fig. 9) although no  $^{23}\text{Na}$  NMR reference spectrum could be found to confirm. The  $^1\text{H}$   
 570  $\rightarrow ^{23}\text{Na}$  CPMAS NMR spectrum does not exactly overlap the MAS spectrum (Fig. 8a). This  
 571 indicates a complex distribution of environments for Na in this powder aged at 40°C, with, in  
 572 average, a more centrosymmetric character (lower mean  $C_Q$ ) and larger Na-O distances (lower  
 573 mean  $\delta_{\text{iso}}$ ) than in the powder aged at 80°C. The  $^1\text{H} \rightarrow ^{23}\text{Na}$  correlated component and the 80°C  
 574 altered glass have very similar  $^{23}\text{Na}$  parameters although (Table 3).

575 In the  $^1\text{H} \rightarrow ^{23}\text{Na}$  HETCOR spectrum in Fig. 8c, the sharp signal is correlated with protons at  
 576 low-frequency only, while the signal of  $\text{Na}^+$  in the hydrated glass is correlated with all the proton  
 577 frequencies, in particular that around +14 ppm consistently with their attribution to OH groups

578 forming hydrogen bonds with NBOs. Thus, Na<sup>+</sup> ions are in close vicinity of all the hydrated  
 579 species (OH and molecular H<sub>2</sub>O) in the glass hydrated at 40°C as well as in the glass hydrated at  
 580 80°C [28]. However, at 40°C, part of the Na<sup>+</sup> ions have migrated and formed carbonates.



581  
 582 **Fig. 8** (a) <sup>23</sup>Na MAS NMR spectra of pristine and bulk altered glass A powder after an ageing at  
 583 80 °C, 85 %RH (32-50 μm, V72h, climatic oven) or at 40 °C, 85 %RH (5-10 μm, V6m, hermetic  
 584 box containing a saline solution of KCl in H<sub>2</sub>O). Spectra are normalized to the same area. (b) Fit  
 585 and decomposition of the spectrum of the 40°C altered powder. (c) HETCOR <sup>1</sup>H → <sup>23</sup>Na  
 586 acquisition with a contact time of 0.8 ms of the 40°C altered powder.  
 587

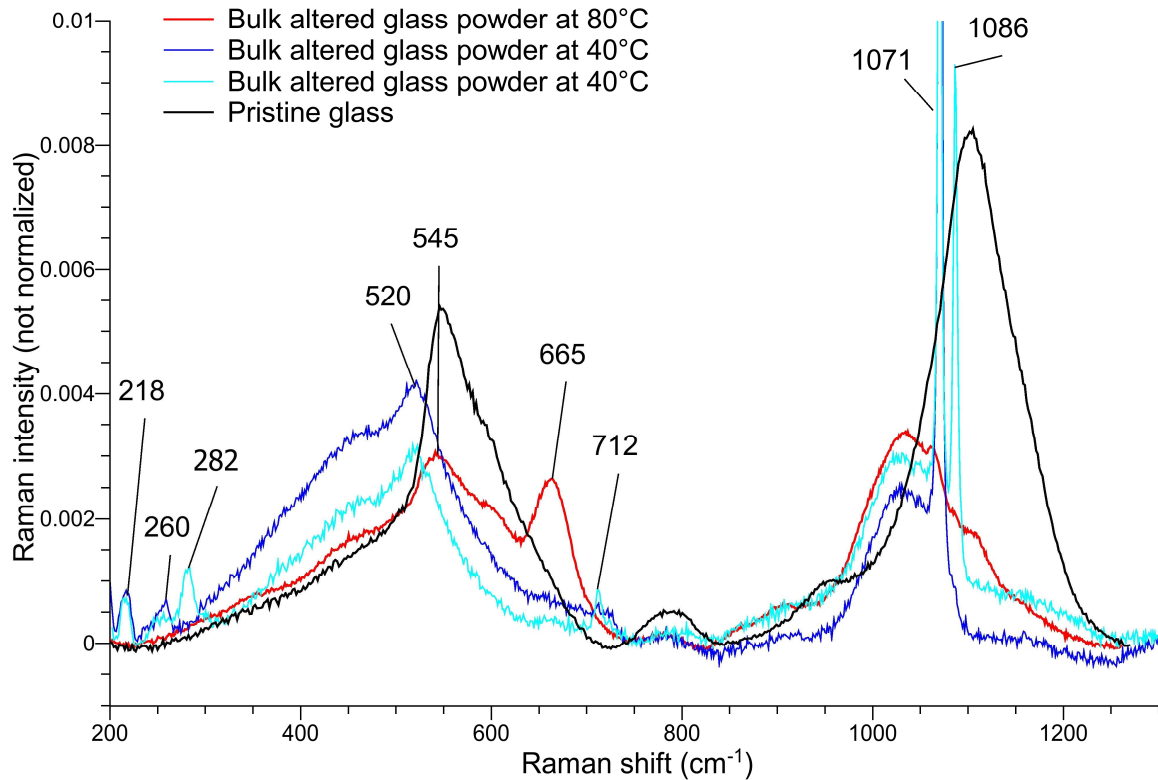
	<sup>23</sup> Na δ <sub>iso</sub>	C <sub>Q</sub> (MHz)	η <sub>Q</sub>	Assignment and proportion
Pristine glass A	+3 (9)	4.3 (1.4)	0.6	
Bulk altered glass 80°C	-1 (4)	1.6 (0.7)	0.6	
Bulk altered glass 40°C MAS	-2.7 (2.3)	1.1 (0.5)	0.6	Large component 50%
	4.8	3.9	0.15	Crystallized component 50%
Bulk altered glass 40°C CP MAS <sup>1</sup> H → <sup>23</sup> Na	-1 (3)	1.8 (0.4)	0.6	

588 **Table 3.** <sup>23</sup>Na NMR fit parameters of the bulk altered glass A powder aged at 40°C. The  
 589 parameters of the pristine glass and 80°C altered powder are also given for comparison.

590  
 591 The Raman spectra of the pristine and bulk altered glass powders are compared in Fig. 9. The  
 592 Raman spectrum of the pristine glass A is typical of alkali silicate glasses with O/Si ratio between  
 593 2.25 (tetrasilicate composition) and 2.5 (disilicate composition), of which silicate network is  
 594 mainly composed of Q<sup>4</sup> and Q<sup>3</sup> units. In the high-frequency range, the band at 1100 cm<sup>-1</sup> is  
 595 assigned to the stretching modes of Q<sup>3</sup> units while the small band at 950 cm<sup>-1</sup> is related to Q<sup>2</sup>  
 596 units [51,52] likely bound to Ca<sup>2+</sup> and Mg<sup>2+</sup> cations [53]. In the intermediate frequency range  
 597 (300-700 cm<sup>-1</sup>), the Raman intensity stems from the Si-O-Si bending modes of the silicate

598 network, and directly reflects the Si-O-Si angle distribution. In alkali silicate glasses, this  
599 distribution is bimodal, with high and widely distributed Si-O-Si angles in polymerized silica-type  
600 regions, and weaker, less distributed Si-O-Si angles in depolymerized sodo-silicate type regions.  
601 The first population is responsible of the broad low-intensity signal around  $460\text{ cm}^{-1}$ , while the  
602 second population gives rise to the peak at  $545\text{ cm}^{-1}$  [54]. The Raman spectra of the bulk altered  
603 glass powders are severely modified. The  $Q^n$  stretching band downshifts to  $1030\text{ cm}^{-1}$  for the two  
604 ageing temperatures  $40^\circ\text{C}$  and  $80^\circ\text{C}$ . The interpretation of the Raman intensity in the  $1020\text{-}1040$   
605  $\text{cm}^{-1}$  range is controversial. Zotov and Keppler assign it to  $Q^3$  species distinct from those causing  
606 the  $1100\text{ cm}^{-1}$  band [55]. Because intensity in this region is present in alkali tectosilicate glasses  
607 [56] and following theoretical results [57], Le Losq et al. ascribe it to asymmetrical stretching of  
608 polymerized units [58]. Considering the NMR results described above on these altered powders,  
609 we prefer the interpretation of Zotov and Kepler and propose to assign this band to  $Q^3$  units  
610 with strong hydrogen bonding of their NBO (these units will be noted  $Q^3(\text{Na,H})$  in this paper). It  
611 is expected that this hydrogen bonding induces a low frequency shift of the  $Q^3$  stretching band,  
612 by weakening the Si-NBO bond. Beside, the well-defined  $Q^2$  peak at  $950\text{ cm}^{-1}$  interestingly  
613 disappears, and a weak intensity signal around  $910\text{ cm}^{-1}$  appears that has been clearly identified as  
614 the stretching mode of Si-OH bonds [55,57]. The decrease of the  $800\text{ cm}^{-1}$  band, ascribed to the  
615 “cage-like” motion of Si in the  $Q^4$  tetrahedron has been observed by Zotov and related to the  
616 depolymerization of the network. The intermediate frequency range shows more variations  
617 according to the ageing temperature. At  $80^\circ\text{C}$ , the Si-O-Si bending band at  $545\text{ cm}^{-1}$  is still  
618 present with a decreased intensity, and a new narrow band at  $665\text{ cm}^{-1}$  has appeared. The  
619 spectrum of the  $80^\circ\text{C}$  altered powder is very close to the spectra of Cultural Heritage glass replica  
620 aged at  $60^\circ\text{C}$  in humid atmosphere with  $100\%$  RH published by Robinet et al. [59]. The narrow  
621 band at  $665\text{-}670\text{ cm}^{-1}$  has been proposed as a characteristic feature of these alteration conditions.  
622 It is assigned to Si-O-Si symmetrical bending in depolymerized and isolated components of the  
623 network, such as  $Q^2$  chains in pyroxenes (of which Si-O-Si bending frequencies are in the range  
624  $650\text{-}700\text{ cm}^{-1}$ ) [60]. Actually, it strongly evokes the intense and characteristic band at  $668\text{-}672\text{ cm}^{-1}$   
625 in calcium silicate hydrate (C-S-H), which consists in  $Q^2$  chains and  $Q^1$  dimers [61]. This  
626 assignment is consistent with the retention of  $\text{Ca}^{2+}$  ions in the hydrated layer at  $80^\circ\text{C}$ . In the  
627 spectra of the powder aged at  $40^\circ\text{C}$ , this peak is absent, and the intensity of the broad band with  
628 maximum at  $460\text{ cm}^{-1}$  has markedly increased, which can be related to partial re-polymerization  
629 of the network. Moreover, the Si-O-Si bending peak originating from the depolymerized  
630 component of the network has shifted to lower frequency, from  $545\text{ cm}^{-1}$  (characteristic of the  
631 NS3 composition [54]) to  $520\text{ cm}^{-1}$  (between NS4 and NS7 composition). This downshift

632 indicates a lower content of alkalis in the altered glass, consistently with the chemical analysis of  
633 the alteration layer that shows a loss of up to 40% of the  $\text{Na}^+$  ions. On the other hand, the sharp  
634 peaks in the spectra of the 40°C altered powder correspond to carbonates, among them calcite  
635 (peaks at 282, 712 and 1086  $\text{cm}^{-1}$ ), gaylussite ( $\text{Na}_2\text{Ca}(\text{CO}_3)_2 \cdot 5\text{H}_2\text{O}$ , peaks at 260 and 1071  $\text{cm}^{-1}$ ),  
636 the peak at 218  $\text{cm}^{-1}$  remaining unidentified.



637  
638 **Fig. 9** Raman spectra of the pristine glass A (black curve) and of bulk altered glass A powder  
639 after an ageing at 80 °C, 85 %RH (32-50  $\mu\text{m}$ , V72h, climatic oven) (red curve) or at 40 °C, 85  
640 %RH (5-10  $\mu\text{m}$ , V6m, hermetic box containing a saline solution of KCl in  $\text{H}_2\text{O}$ ). Because of the  
641 presence of carbonates in the powder aged at 40°C, there is a variability in the Raman spectra, so  
642 that two spectra are shown for this powder (blue and cyan curves).

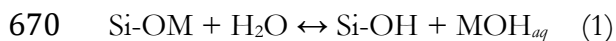
643

#### 644 4. DISCUSSION

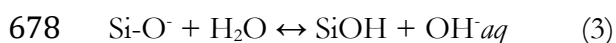
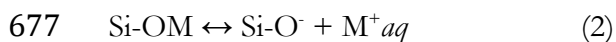
645 The alteration layer produced in glass A in atmospheric conditions (85 %RH) is composed of a  
646 hydrated layer with no depletion of any chemical element at 80°C, and of a hydrated layer  
647 depleted in Ca (totally) and Na (partially) with carbonate salts on the surface at 40°C. The  
648 concentration of tightly bound water is about 5 to 10 wt% with no clear indication of a different  
649 water content at 80°C and at 40°C. This water is present as molecular  $\text{H}_2\text{O}$  and as Si-OH species  
650 with a wide distribution of H-bonding strengths, the strongest ones connecting H to NBO's like  
651 in alkali silicate hydrates. From  $^{29}\text{Si}$  NMR and Raman spectra, the silicate network has

652 depolymerized with the ageing and bears primarily Q<sup>3</sup>-H (Si-OH) and Q<sup>3</sup>-M,H (Si-OM---H with  
653 M = Na or K) units, although at 40°C a part of the network has also re-polymerized, possibly  
654 after the departure of some Na<sup>+</sup> and Ca<sup>2+</sup> ions. We emphasize that the structure of the hydrated  
655 layer produced in these atmospheric conditions markedly differs from the structure of the  
656 alteration layer, often called « alteration gel », produced in immersion conditions. In the latter  
657 conditions, the gel is completely depleted in alkalis and the silicate network has re-polymerized,  
658 following either *in situ* condensation reactions or silica precipitation from the solution [62]. In  
659 atmospheric conditions, the hydrated glass still contains a significant amount of alkalis and  
660 NBO's, and is closer to an alkali silicate hydrate than to an alteration gel. As in hydrates, the  
661 dense network of hydrogen bonds probably contributes to the stability of the layer [63].

662 In the hydrated layer, Na<sup>+</sup> ions are surrounded by NBO's, OH groups and molecular water as  
663 inferred from the <sup>1</sup>H → <sup>23</sup>Na CP NMR spectra. They are thus totally or partially solvated  
664 explaining that they are finally detached from the NBO's and leached out of the glass. There is  
665 no structural information on the environment of K<sup>+</sup> and Ca<sup>2+</sup>, but because leaching of K<sup>+</sup> is  
666 never observed in these experiments, we may propose that K<sup>+</sup> ions are still primarily bound to  
667 NBO's in the hydrated glass. On the contrary, at 40°C, Ca<sup>2+</sup> ions are primarily solvated because  
668 they are totally leached out, forming carbonates on the glass surface. These observations can be  
669 summarized by considering the following equilibrium in the hydrated glass:



671 Where M are alkali (Na<sup>+</sup> or K<sup>+</sup>) or half a Ca<sup>2+</sup> ion and *aq* refers to the hydrated state of MOH.  
672 This well-known equilibrium has been referred to as « ion exchange » [64] but it is more exactly  
673 an acid-base reaction of water with the NBO sites, implying diffusion of molecular water and its  
674 immobilization by the formation of silanol groups [65,66]. It can also be viewed as a  
675 complexation equilibrium of the M cations with the silicate polyanionic network, associated to  
676 the acid-base reaction ((1) = (2)+(3)) :



679 Reaction (2) points out the fact that there is a balance between the solvation (or hydration) of the  
680 M<sup>+</sup> cations and their inner sphere complexation on the silicate NBO sites. A similar balance  
681 governs the selectivity of clays for alkali ions and results in the order Cs<sup>+</sup> > K<sup>+</sup> > Na<sup>+</sup> > Li<sup>+</sup>,  
682 because the energy of hydration that goes in the reverse order overrides the energy of  
683 complexation in the interlayer (Teppen and Miller, 2006; Rotenberg et al., 2009). Similar ionic  
684 selectivity has been found in the alteration gels of the International Simple Glass (ISG) formed in  
685 Si-saturated solutions with increasing alkali salts concentrations : the K<sup>+</sup> or Cs<sup>+</sup> ions provided by

686 the solution almost totally substitute the  $\text{Ca}^{2+}$  ions in the gels, while  $\text{Na}^+$  and  $\text{Li}^+$  ions do not [69].  
687 The authors interpreted these results by analogy with the selectivity in clays, suggesting that it is  
688 mainly determined by the affinity of cations for hydration, rather than for pore surface  
689 complexation:  $\text{K}^+$  and  $\text{Cs}^+$  are “hydrophobic” cations that prefer complexation. We propose to  
690 use the same analogy to explain our observation that cationic species are detached of the NBO’s  
691 in the order  $\text{Na}^+ > \text{K}^+$ .  $\text{Na}^+$  ions are more stabilized by solvation than  $\text{K}^+$  and are thus more  
692 quantitatively converted to solvated species, able to migrate under a chemical potential gradient.  
693 Moreover, in alkali disilicate hydrates,  $\text{K}^+$  are not coordinated to molecular  $\text{H}_2\text{O}$  and form  
694 “ $\text{KHSi}_2\text{O}_5$ ” units, while  $\text{Na}^+$  are coordinated to NBO *and*  $\text{H}_2\text{O}$  [39]. It is then possible that Si-  
695 OK units are particularly stabilized in the H-bonding network, adding another energy term  
696 favouring the left side of reaction (2). Concerning  $\text{Ca}^{2+}$  ions, their observed behaviour is striking  
697 as it is very contrasted with the temperature, revealing both the specificity of atmospheric  
698 alteration phenomena and the temperature-induced change in their mechanisms. At  $80^\circ\text{C}$ , the  
699  $\text{Ca}^{2+}$  ions remain in the alteration layer and locally form C-S-H-type structures evidenced by the  
700  $665\text{ cm}^{-1}$  sharp band in the Raman spectra. At  $40^\circ\text{C}$  on the contrary,  $\text{Ca}^{2+}$  ions are totally leached  
701 out of the alteration layer, forming calcium carbonates on the surface. This behaviour is in  
702 contrast to the one expected considering the calcite solubility, which decreases when temperature  
703 rises. The hydration energy of  $\text{Ca}^{2+}$  is three times that of  $\text{Na}^+$  so that  $\text{Ca}^{2+}$  are markedly stabilized  
704 by hydration [70]. Following the preceding discussion, this probably explains that  $\text{Ca}^{2+}$  ions are  
705 more quantitatively extracted out of the hydrated layer than  $\text{Na}^+$  at  $40^\circ\text{C}$ . Because the enthalpies  
706 of hydration and complexation are likely both modest, the dominance of the hydration term is  
707 expected to be similar at  $40^\circ\text{C}$  and at  $80^\circ\text{C}$ . So, why aren’t  $\text{Ca}^{2+}$  ions (and  $\text{Na}^+$  ions) also  
708 extracted at  $80^\circ\text{C}$ ? To answer this question, we consider the specificity of atmospheric alteration  
709 that lies in the scarcity of water with respect to the silicate solid phase. In the first stage of the  
710 alteration, it may be assumed that all the water molecules are bound to the surface or within the  
711 hydrated layer, consequently losing part of their solvating properties. Such an effect has been  
712 observed in several molecular dynamics simulations of water confined in silica nanopores [71–  
713 73]. Then, the complete solvation of the  $\text{M}^+$  ion and its detachment from the NBO may be  
714 considerably slowed down. If water molecules are engaged in another reaction as the Si-O-Si  
715 bond hydrolysis, as proposed below, then the  $\text{M}^+$  ions may never be completely solvated and  
716 extracted.

717 Next to the acid-base reaction on the NBO sites (reaction (1)), there is another reaction called  
718 hydrolysis of the Si-O-Si bonds:



720 This reaction *only* is responsible for the silicate network depolymerisation when shifted to the  
721 right. It is well-known that this reaction can be catalysed either by protonic assistance (acid pH)  
722 or by nucleophilic attack by OH<sup>-</sup> ions (basic pH). The activation energy of this reaction is high  
723 (86 kJ.mol<sup>-1</sup> according to [34]) and certainly higher than the activation energy for hydration.  
724 Therefore, this reaction is considerably enhanced with temperature, going much faster to the  
725 right at 80°C with respect to 40°C. This provides the basis of our hypothesis to explain the  
726 different phenomena observed for atmospheric alteration of glass A at 80°C and at 40°C. Indeed,  
727 in addition to the different behaviour of Na<sup>+</sup> and Ca<sup>2+</sup> cations described above, there is a  
728 considerable temperature-induced increase of the kinetics of the glass hydration, as measured by  
729 the growth of the hydrated, depolymerized layer. We propose that it is due to the increase of the  
730 rate of the hydrolysis reaction (4), relatively to the rate of reaction (1). Water molecules are  
731 primarily engaged in network hydrolysis rather than in acid-base dissociation onto NBO sites at  
732 80°C. On the contrary at 40°C, the rates of the two reactions converge and water molecules  
733 have the time to solvate M<sup>+</sup> and OH<sup>-</sup> ions that then migrate towards the surface to form  
734 carbonates. Note that Si-O-Si hydrolysis, instead of acid-base dissociation has been inferred from  
735 the study of the hydration process of sodium disilicate, forming Q<sup>2</sup> [(SiO)<sub>2</sub>Si-(OH)O<sup>-</sup>Na<sup>+</sup>] rather  
736 than Q<sup>3</sup> [(SiO)<sub>3</sub>Si-OH] groups. The authors suggested a possible stabilization of these Q<sup>2</sup> groups  
737 by the strong H-bonding [63].

738 Another striking feature of the atmospheric alteration of glass A is the acceleration of the  
739 kinetics, observed both at 80°C and at 40°C. The simple “diffusion control” or “surface control”  
740 models cannot account for this complex kinetics. Given our understanding of the alteration  
741 phenomena described above, the network hydrolysis (reaction (4)) is the rate-controlling step at  
742 least at 80°C. This reaction is accelerating with the ageing time and hydrated layer thickness (in  
743 the timescale of our experiments). Wang et al. have highlighted the existence of self-accelerating  
744 mechanisms in the aqueous alteration of silicate glasses, due to the catalytic effect of OH<sup>-</sup> ions  
745 that are released by the acid-base reaction step [74,75]. We propose that this effect also operates  
746 in atmospheric conditions. After a time period depending on the availability and solvation  
747 properties of water in the hydrated layer, M<sup>+</sup> and OH<sup>-</sup> ions end up being released and catalyse the  
748 network hydrolysis, accelerating the glass hydration rate. It is probable that OH<sup>-</sup> ions stay trapped  
749 in the H bonding network, as well as their precursor form NBO+H<sub>2</sub>O, and that both species  
750 contribute to the acceleration of the Si-O-Si bond hydrolysis.

751 At last, we have attempted to rationalize our observations of the atmospheric alteration  
752 phenomenology of glass A using a molecular-scale approach based on the relative rates of  
753 reactions (1) and (4). This also corresponds to the basis of the incongruent dissolution model for

754 glasses [76]. Two considerations have been added: the important role of the hydration of cations,  
755 and the bound or *ice-like* character of water molecules due to their confinement and scarcity.  
756 These considerations are very recent in the glass alteration community. On the other hand, an  
757 alternative model for glass dissolution has been proposed on the basis of the very sharp interface  
758 between the gel and the pristine glass. It consists in the coupling of surface congruent dissolution  
759 and precipitation at the interface (CIDP for Coupled Interface Dissolution Precipitation) [32].  
760 We also observe many features that evoke CIDP, as the sharpness of the interface evidenced by  
761 the flaking phenomenon and the chemical homogeneity of the hydrated layer. However, we think  
762 that the molecular aspects that we have discussed, because they occur at the molecular scale near  
763 the alteration front, are relevant to both models. It is possible that the properties of confined  
764 water specific to atmospheric conditions preclude any meaningful distinction between the two  
765 descriptions of glass alteration.

766

## 767 5. CONCLUSION

768 In this study, the atmospheric alteration (RH = 85 %) of a mixed alkali lime silicate glass  
769 representative of a family of unstable compositions of the Cultural Heritage has been described  
770 in detail as a function of temperature and time. It is the first time that compositional information  
771 on the hydrated layer is accompanied by structural data (multinuclear NMR and Raman  
772 spectroscopies) obtained on bulk altered glass powders. First, this study provides a clear evidence  
773 that in atmospheric conditions, the hydrolysis of the silicate network (Si-O-Si bonds) is mainly  
774 responsible for the glass hydration and controls its kinetics. The leaching of alkali and alkaline-  
775 earth cations is limited, probably because of the scarcity and tightly H-bonded character of water,  
776 which diminish its solvation property. At 40°C, the cations are leached in the order  $\text{Ca}^{2+} > \text{Na}^+$   
777  $\gg \text{K}^+$ , possibly revealing the role of the hydration energy in the leaching process. At 80°C, no  
778 leaching is even observed and the hydration by network hydrolysis occurs very rapidly. The  
779 thermally activated character of hydrolysis induces an acceleration of this process with respect to  
780 other processes (acid-base dissociation of water on NBO sites, cation solvation, cation migration  
781 towards the surface). In addition, we suggest that the time acceleration of the hydration kinetics  
782 at both temperatures points out another effect: the self-accelerating property of the system  
783 towards hydrolysis, due to the catalytic effect of the  $\text{OH}^-$  ions trapped in the H-bonding network,  
784 or of their precursor  $\text{H}_2\text{O}$  species that are H-bonded to NBOs. This effect may contribute to the  
785 very strong temperature dependency of the hydration kinetics, because at 80°C more NBOs and  
786 alkalis are retained in the layer. As a consequence of the partial alkali retention and network  
787 depolymerization, the hydrated layer structure is closer to an unstable alkali silicate hydrate than

788 to an alteration gel (as produced in immersion conditions), at least in the first stages of the  
789 alteration. This knowledge is important in the research for efficient surface chemical treatments  
790 aimed at preventing glass objects from atmospheric degradation in museum collections.

791

## 792 **DATA AVAILABILITY**

793 The raw data required to reproduce these findings are available to download from Mendeley  
794 Dataset <http://dx.doi.org/10.17632/mnjkhzr6sx.3>.

795

## 796 **REFERENCES**

- 797 [1] T. Lombardo, L. Gentaz, A. Verney-Carron, A. Chabas, C. Loisel, D. Neff, E. Leroy,  
798 Characterisation of complex alteration layers in medieval glasses, *Corros. Sci.* 72 (2013)  
799 10–19. doi:10.1016/j.corsci.2013.02.004.
- 800 [2] M. Melcher, M. Schreiner, Leaching studies on naturally weathered potash-lime–silica  
801 glasses, *J. Non. Cryst. Solids.* 352 (2006) 368–379. doi:10.1016/j.jnoncrysol.2006.01.017.
- 802 [3] P. Bellendorf, H. Roemich, S. Gerlach, P. Mottner, E. López, K. Wittstadt, Archaeological  
803 glass: the surface and beyond, *Glas. Ceram. Conserv. 2010 Interim Meet. ICOM-CC*  
804 *Work. Group*, Oct. 3-6 2010 Corning, New York, U.S.A. (2010) 137–144.
- 805 [4] J.J. Kunicki-Goldfinger, Unstable historic glass : symptoms, causes, mechanisms and  
806 conservation, *Rev. Conserv.* 9 (2008) 47–60.
- 807 [5] S.P. Koob, *Conservation and care of glass objects*, Archetype, New-York, 2006.
- 808 [6] M. Melcher, M. Schreiner, Glass degradation by liquids and atmospheric agents, in: J.K.H.  
809 A. (Ed.), *Mod. Methods Fo Anal. Archeol. Hist. Glas.*, Wiley, 2013: pp. 608–651.
- 810 [7] R.H. Brill, The morphology of weathering on historical glasses, *Riv. Della Stn. Sper. Del*  
811 *Vetro Sper. Del Vetro.* 6 (2000) 7–8.
- 812 [8] L. Robinet, *The role of organic pollutants in the alteration of historic soda silicate glasses*,  
813 *Edinburgh - Paris VI*, 2006.
- 814 [9] R.M. Organ, The safe storage of unstable glass, *Museums J.* 56 (1957) 255–272.
- 815 [10] R.H. Brill, Crizzling - A Problem in Glass Conservation, in: *Conserv. Archeol. Appl. Arts*,  
816 *Stock. Congr. 2-6 June 1975*, International Institute for Conservation, London, 1975: pp.  
817 121–124.
- 818 [11] S.P. Koob, Crizzling glasses : problems and solutions, *Eur. J. Glas. Sci. Technol. A.* 53  
819 (2012) 225–227.
- 820 [12] V. Oakley, Fighting the inevitable : the continuing search for a solution to glass decay at  
821 the V&A, *Glas. Technol.* 42 (2001) 65–69.

- 822 <http://cat.inist.fr/?aModele=afficheN&cpsidt=14078296> (accessed November 16, 2014).
- 823 [13] S. Davison, R.G. Newton, *Conservation and restauration of glass*, Butterworth, 2003.
- 824 [14] M. Verità, R. Falcone, G. Sommariva, M.H. Chopinet, P. Lehuédé, Weathering of the  
825 inner surface of soda-lime-silica glass containers exposed to the atmosphere, *Glas.*  
826 *Technol. Eur. J. Glas. Sci. Technol. Part A.* 50 (2009) 65–70.
- 827 [15] M.-H. Chopinet, P. Lehuédé, Les problèmes d'altération rencontrés sur des verres  
828 industriels, *Verre.* 16 (2010) 20–27.
- 829 [16] M.-H. Chopinet, M. Verità, R. Falcone, P. Lehuédé, M. Vallotto, M. Nardone, A. Sodo,  
830 Soda-lime-silica glass containers: chemical durability and weathering products, *Adv. Mater.*  
831 *Res.* 39–40 (2008) 305–310. doi:10.4028/www.scientific.net/AMR.39-40.305.
- 832 [17] C. Wang, G. Krausch, E. Rädlein, S. Tratzky, M. Schramm, A. Weber, Study of surface  
833 changes on industrial glasses with AFM, FE-SEM, EDX, SNMS and LM, *Glas. Sci.*  
834 *Technol.* 6 (2004) 273–282.
- 835 [18] A.A. Chaou, A. Abdelouas, Y. El Mendili, R. Bouakkaz, S. Utsunomiya, C. Martin, X.  
836 Bourbon, Vapor hydration of a simulated borosilicate nuclear waste glass in unsaturated  
837 conditions at 50°C and 90°C, *RSC Adv.* 5 (2015) 64538–64549.
- 838 [19] T.A. Abrajano, J.K. Bates, J.J. Mazer, Aqueous corrosion of natural and nuclear waste  
839 glasses II. Mechanisms of vapor hydration of nuclear waste glasses, *J. Non. Cryst. Solids.*  
840 108 (1989) 269–288. doi:10.1016/0022-3093(89)90297-4.
- 841 [20] R. Bouakkaz, A. Abdelouas, A.A. Chaou, Y. El Mendili, A borosilicate glass hydration at  
842 low temperature, *J. Chem. Pharm. Res.* 7 (2015) 332–337.
- 843 [21] M. Verità, Modern and ancient glass: nature, composition and deterioration mechanisms,  
844 in: R.-A. Lefèvre (Ed.), *Mater. Cult. Herit. Their Environ.*, Edipuglia, Bari, 2006: pp. 119–  
845 132.
- 846 [22] R. Falcone, F. Licenziati, E.F. Orsega, M. Verità, The dependence of the weathering of  
847 soda-lime-silica glass on environmental parameters: A preliminary investigation, *Eur. J.*  
848 *Glas. Sci. Technol. Part A.* 52 (2011) 23–29.
- 849 [23] L. Robinet, C. Hall, K. Eremin, S. Fearn, J. Tate, Alteration of soda silicate glasses by  
850 organic pollutants in museums: Mechanisms and kinetics, *J. Non. Cryst. Solids.* 355 (2009)  
851 1479–1488. doi:10.1016/j.jnoncrysol.2009.05.011.
- 852 [24] S. Fearn, D.S. McPhail, B. Hagenhoff, E. Tallarek, TOF-SIMS analysis of corroding  
853 museum glass, *Appl. Surf. Sci.* 252 (2006) 7136–7139. doi:10.1016/j.apsusc.2006.02.157.
- 854 [25] A. Rodrigues, S. Fearn, M. Vilarigues, Historic K-rich silicate glass surface alteration:  
855 Behaviour of high-silica content matrices, *Corros. Sci.* 145 (2018) 249–261.

- 856 doi:10.1016/j.corsci.2018.10.010.
- 857 [26] A. Rodrigues, S. Fearn, T. Palomar, M. Vilarigues, Early stages of surface alteration of  
858 soda-rich-silicate glasses in the museum environment, *Corros. Sci.* 143 (2018) 362–375.  
859 doi:10.1016/j.corsci.2018.08.012.
- 860 [27] I. Biron, *Émaux sur Métal – du IXe au XIXe Siècle. Histoire, Technique et Matériaux*,  
861 Faton, 2015.
- 862 [28] F. Alloteau, P. Lehuédé, O. Majérus, T. Charpentier, D. Caurant, I. Biron, New insight  
863 into atmospheric alteration of alkali-lime silicate glasses, *Corros. Sci.* 122 (2017) 12–25.  
864 doi:10.1016/j.corsci.2017.03.025.
- 865 [29] L. Greenspan, Humidity fixed points of binary saturated aqueous solutions, *J. Res. Natl.*  
866 *Bur. Stand. Sect. A Phys. Chem.* 81A (1977) 89. doi:10.6028/jres.081A.011.
- 867 [30] L.R. Riciputi, J.. M. Elam, L.M. Anovitz, D.R. Cole, Obsidian diffusion dating by  
868 secondary ion mass spectrometry: A test using results from Mound 65, Chalco, Mexico, *J.*  
869 *Archaeol. Sci.* 29 (2002) 1055–1075. doi:10.1006/jasc.2001.0692.
- 870 [31] F.M. Ernsberger, Properties of glass surfaces, *Annu. Rev. Mater. Sci.* 2 (1972) 529–572.
- 871 [32] C. Lenting, O. Plümper, M. Kilburn, P. Guagliardo, M. Klinkenberg, Towards a unifying  
872 mechanistic model for silicate glass corrosion, *Npj Mater. Degrad.* 28 (2018).  
873 doi:10.1038/s41529-018-0048-z.
- 874 [33] H. Scholze, Chemical durability of glasses, *J. Non. Cryst. Solids.* 52 (1982) 91–103.
- 875 [34] A. Verney-Carron, S. Gin, P. Frugier, G. Libourel, Long-term modeling of alteration-  
876 transport coupling: Application to a fractured Roman glass, *Geochim. Cosmochim. Acta.*  
877 74 (2010) 2291–2315. doi:10.1016/j.gca.2010.01.001.
- 878 [35] X. Xue, M. Kanzaki, Proton distributions and hydrogen bonding in crystalline and glassy  
879 hydrous silicates and related inorganic materials: Insights from high-resolution solid-state  
880 nuclear magnetic resonance spectroscopy, *J. Am. Ceram. Soc.* 92 (2009) 2803–2830.  
881 doi:10.1111/j.1551-2916.2009.03468.x.
- 882 [36] T. Schaller, A. Sebald, One- and two-dimensional <sup>1</sup>H magic-angle spinning experiments  
883 on hydrous silicate glasses, *Solid State Nucl. Magn. Reson.* 5 (1995) 89–102.  
884 doi:10.1016/0926-2040(95)00028-O.
- 885 [37] H. Eckert, J.P. Yesinowski, L.A. Silver, E.M. Stolper, Water in silicate glasses: quantitation  
886 and structural studies by proton solid echo and magic angle spinning NMR methods, *J.*  
887 *Phys. Chem.* 92 (1988) 2055–2064. doi:10.1021/j100318a070.
- 888 [38] X. Ai, F. Deng, J. Dong, W. Hu, H. Xu, C. Ye, One- and two-dimensional solid-state  
889 magic angle spinning NMR studies on the hydration process of layered sodium disilicate

890 SKS-6., *Solid State Nucl. Magn. Reson.* 25 (2004) 216–26.  
891 doi:10.1016/j.ssnmr.2003.10.002.

892 [39] G.G. Almond, R.K. Harris, K.R. Franklin, A structural consideration of kanemite,  
893 octosilicate, magadiite and kenyaite, *J. Mater. Chem.* 7 (1997) 681–687.  
894 doi:10.1039/a606856a.

895 [40] X. Xue, M. Kanzaki, Dissolution mechanisms of water in depolymerized silicate melts:  
896 Constraints from  $^1\text{H}$  and  $^{29}\text{Si}$  NMR spectroscopy and ab initio calculations, *Geochim.*  
897 *Cosmochim. Acta.* 68 (2004) 5027–5057. doi:10.1016/j.gca.2004.08.016.

898 [41] C. Le Losq, G.D. Cody, B.O. Mysen, Alkali influence on the water speciation and the  
899 environment of protons in silicate glasses revealed by  $^1\text{H}$  MAS NMR spectroscopy, *Am.*  
900 *Mineral.* 100 (2015) 466–473. doi:10.2138/am-2015-5004.

901 [42] E. Robert, A. Whittington, F. Fayon, M. Pichavant, D. Massiot, Structural characterization  
902 of water-bearing silicate and aluminosilicate glasses by high-resolution solid-state NMR,  
903 *Chem. Geol.* 174 (2001) 291–305. doi:10.1016/S0009-2541(00)00321-1.

904 [43] S.C. Kohn, R. Dupree, M.E. Smith, Proton environments and hydrogen-bonding in  
905 hydrous silicate glasses from proton NMR, *Nature.* 337 (1989) 539–541.  
906 doi:10.1038/337539a0.

907 [44] F. Angeli, M. Gaillard, P. Jollivet, T. Charpentier, Influence of glass composition and  
908 alteration solution on leached silicate glass structure: A solid-state NMR investigation,  
909 *Geochim. Cosmochim. Acta.* 70 (2006) 2577–2590. doi:10.1016/j.gca.2006.02.023.

910 [45] C. Gardienet, P. Tekely, Structural and Motional Features of a Layered Sodium Hydrous  
911 Silicate as Revealed by Solid State NMR, *J. Phys. Chem. B.* 106 (2002) 8928–8936.

912 [46] H. Maekawa, T. Maekawa, K. Kawamura, T. Yokokawa, The structural groups of alkali  
913 silicate glasses determined from  $^{29}\text{Si}$  NMR, *J. Non. Cryst. Solids.* 127 (1991) 53–64.

914 [47] D.R. Spearing, I. Farnan, J.F. Stebbins, Dynamics of the  $\alpha$ - $\beta$  phase transitions in quartz  
915 and cristobalite as observed by in-situ high temperature  $^{29}\text{Si}$  and  $^{17}\text{O}$  NMR, *Phys. Chem.*  
916 *Miner.* 19 (1992) 307–321. doi:10.1007/BF00204008.

917 [48] F. Angeli, O. Villain, S. Schuller, S. Ispas, T. Charpentier, Insight into sodium silicate glass  
918 structural organization by multinuclear NMR combined with first-principles calculations,  
919 *Geochim. Cosmochim. Acta.* 75 (2011) 2453–2469. doi:10.1016/j.gca.2011.02.003.

920 [49] F. Angeli, J.M. Delaye, T. Charpentier, J.-C. Petit, D. Ghaleb, P. Faucon, Influence of  
921 glass chemical composition on the Na-O bond distance: a  $^{23}\text{Na}$  3Q-MAS NMR and  
922 molecular dynamics study, *J. Non. Cryst. Solids.* 276 (2000) 132–144.  
923 doi:10.1097/00001756-200112210-00023.

- 924 [50] F. Angeli, M. Gaillard, P. Jollivet, T. Charpentier, Ca MAS NMR for probing the structural  
925 configuration of calcium in glass, *Chem. Phys. Lett.* 440 (2007) 324–328.  
926 doi:10.1016/j.cplett.2007.04.036.
- 927 [51] T. Furukawa, K.E. Fox, W.B. White, Raman spectroscopic investigation of the structure  
928 of silicate glasses. III. Raman intensities and structural units in sodium silicate glasses, *J.*  
929 *Chem. Phys.* 75 (1981) 3226–3237. doi:10.1063/1.442472.
- 930 [52] P. Mcmillan, Structural studies of silicate glasses and melts-applications and limitations of  
931 Raman spectroscopy, *Am. Mineral.* 69 (1984) 622–644.
- 932 [53] L. Robinet, C. Coupry, K. Eremin, C. Hall, The use of Raman spectrometry to predict the  
933 stability of historic glasses, *J. Raman Spectrosc.* 37 (2006) 789–797. doi:10.1002/jrs.1540.
- 934 [54] B. Hehlen, D.R. Neuville, D. Kilymis, S. Ispas, Bimodal distribution of Si–O–Si angles in  
935 sodo-silicate glasses, *J. Non. Cryst. Solids.* 469 (2017) 39–44.  
936 doi:10.1016/j.jnoncrysol.2017.04.009.
- 937 [55] N. Zotov, H. Keppler, The influence of water on the structure of hydrous sodium  
938 tetrasilicate glasses, *Am. Miner.* 83 (1998) 823–834. doi:scopus/2-s2.0-0031797062.
- 939 [56] C. Le Losq, D.R. Neuville, Effect of the Na/K mixing on the structure and the rheology  
940 of tectosilicate silica-rich melts, *Chem. Geol.* 346 (2013) 57–71.  
941 doi:10.1016/j.chemgeo.2012.09.009.
- 942 [57] G. Spiekermann, M. Steele-Macinnis, C. Schmidt, S. Jahn, Vibrational mode frequencies of  
943 silica species in SiO<sub>2</sub>-H<sub>2</sub>O liquids and glasses from ab initio molecular dynamics, *J.*  
944 *Chem. Phys.* 136 (2012). doi:10.1063/1.3703667.
- 945 [58] C. Le Losq, B.O. Mysen, G.D. Cody, Water and magmas: insights about the water  
946 solution mechanisms in alkali silicate melts from infrared, Raman, and <sup>29</sup>Si solid-state  
947 NMR spectroscopies, *Prog. Earth Planet. Sci.* 2 (2015). doi:10.1186/s40645-015-0052-7.
- 948 [59] L. Robinet, K. Eremin, C. Coupry, C. Hall, N. Lacombe, Effect of organic acid vapors on  
949 the alteration of soda silicate glass, *J. Non. Cryst. Solids.* 353 (2007) 1546–1559.  
950 doi:10.1016/j.jnoncrysol.2007.01.039.
- 951 [60] H. Ohashi, M. Sekita, Raman Spectroscopic Study of the Si-O-Si Stretching Vibration in  
952 Clinopyroxenes, *J. Japan Assoc. Mineral. Petrol. Sci.* 77 (1982) 455–459.
- 953 [61] C. Breen, K. Garbev, J. Yarwood, B. Gasharova, P. Stemmermann, L. Black, Structural  
954 Features of C<sub>2</sub>S<sub>2</sub>H(I) and Its Carbonation in Air? A Raman Spectroscopic Study. Part I:  
955 Fresh Phases, *J. Am. Ceram. Soc.* 90 (2007) 900–907. doi:10.1111/j.1551-  
956 2916.2006.01428.x.
- 957 [62] F. Angéli, M. Gaillard, P. Jollivet, T. Charpentier, Influence of glass composition and

958 alteration solution on leached silicate glass structure: A solid-state NMR investigation,  
959 *Geochim. Cosmochim. Acta.* 70 (2006) 2577–2590. doi:10.1016/j.gca.2006.02.023.

960 [63] X. Ai, F. Deng, J. Dong, L. Chen, C. Ye, Stability of layered sodium disilicate during  
961 hydration process as studied by multinuclear solid state NMR spectroscopy, *J. Phys.*  
962 *Chem. B.* 106 (2002) 9237–9244. doi:10.1021/jp020458i.

963 [64] B.C. Bunker, Molecular mechanisms for corrosion of silica and silicate glasses, *J. Non.*  
964 *Cryst. Solids.* 179 (1994) 300–308. doi:10.1016/0022-3093(94)90708-0.

965 [65] B.M.J. Smets, T.P.A. Lommen, The role of molecular water in the leaching of glass, *Phys.*  
966 *Chem. Glas.* 24 (1983) 35–36.

967 [66] B.M.J. Smets, On the mechanism of the corrosion of glass by water, *Philips Tech. Rev.* 42  
968 (1985) 59–64.

969 [67] B.J. Teppen, D.M. Miller, Hydration Energy Determines Isovalent Cation Exchange  
970 Selectivity by Clay Minerals, *Soil Sci. Soc. Am. J.* 70 (2006) 31–40.

971 [68] B. Rotenberg, J.P. Morel, V. Marry, P. Turq, N. Morel-Desrosiers, On the driving force of  
972 cation exchange in clays: Insights from combined microcalorimetry experiments and  
973 molecular simulation, *Geochim. Cosmochim. Acta.* 73 (2009) 4034–4044.  
974 doi:10.1016/j.gca.2009.04.012.

975 [69] M. Collin, M. Fournier, T. Charpentier, M. Moskura, S. Gin, Impact of alkali on the  
976 passivation of silicate glass, *Npj Mater. Degrad.* 2 (2018) 16. doi:10.1038/s41529-018-  
977 0036-3.

978 [70] Y. Marcus, Thermodynamics of Solvation of Ions. Part 5. Gibbs free energy of hydration  
979 at 298.15 K, *J. Chem. Soc. Faraday Trans.* 87 (1991) 2995–2999.  
980 doi:10.1524/zpch.1992.176.part\_1.130.

981 [71] M. Collin, S. Gin, B. Dazas, T. Mahadevan, J. Du, I.C. Bourg, Molecular Dynamics  
982 Simulations of Water Structure and Diffusion in a 1 nm Diameter Silica Nanopore as a  
983 Function of Surface Charge and Alkali Metal Counterion Identity, *J. Phys. Chem. C.* 122  
984 (2018) 17764–17776. doi:10.1021/acs.jpcc.8b03902.

985 [72] I.C. Bourg, C.I. Steefel, Molecular dynamics simulations of water structure and diffusion  
986 in silica nanopores, *J. Phys. Chem. C.* 116 (2012) 11556–11564. doi:10.1021/jp301299a.

987 [73] S. Senapati, A. Chandra, Dielectric constant of water confined in a nanocavity, *J. Phys.*  
988 *Chem. B.* 105 (2001) 5106–5109. doi:10.1021/jp011058i.

989 [74] Y. Wang, C.F. Jove-Colon, C. Lenting, J. Icenhower, K.L. Kuhlman, Morphological  
990 instability of aqueous dissolution of silicate glasses and minerals, *Npj Mater. Degrad.* 2  
991 (2018) 27. doi:10.1038/s41529-018-0047-0.

992 [75] Y. Wang, C.F. Jove-Colon, K.L. Kuhlman, Nonlinear dynamics and instability of aqueous  
993 dissolution of silicate glasses and minerals, *Sci. Rep.* 6 (2015) 30256. doi:10.1038/s41529-  
994 018-0047-0.

995 [76] S. Gin, L. Neill, M. Fournier, P. Frugier, T. Ducasse, M. Tribet, A. Abdelouas, B. Parruzot,  
996 J. Neeway, N. Wall, The controversial role of inter-diffusion in glass alteration, *Chem.*  
997 *Geol.* 440 (2016) 115–123. doi:10.1016/j.chemgeo.2016.07.014.

998

#### 999 **ACKNOWLEDGEMENTS**

1000 The authors gratefully thank PSL University for the funding of this work, Marie-Hélène  
1001 Chopinet, Sophie Papin and Kamila Plevacova (Saint-Gobain Recherche, France) for the glass  
1002 fabrication. Mélanie Moskura (NIMBE, CEA) is acknowledged for her help in conducting the  
1003 NMR experiments.

1004

#### 1005 **SUPPLEMENTARY MATERIALS**

1006 See Data in Brief zip file.